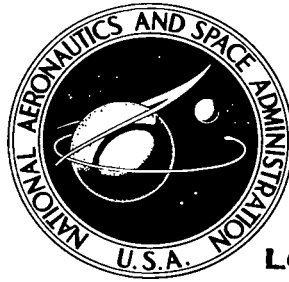


NASA TECHNICAL NOTE

NASA TN D-8356



NASA TN D-8356

C.1

LOAN COPY:  
AFWL TECHNIC  
KIRTLAND A



TO  
PAR  
M.

## ELECTRON DYNAMICS IN A PLASMA FOCUS

*Frank Hohl, S. Peter Gary,  
and Patricia A. Winters*

*Langley Research Center  
Hampton, Va. 23665*



0134062

1. Report No. NASA TN D-8356		2. Government Accession No.		3. Recipient's Catalog No.	
4. Title and Subtitle ELECTRON DYNAMICS IN A PLASMA FOCUS				5. Report Date February 1977	
				6. Performing Organization Code	
7. Author(s) Frank Hohl, S. Peter Gary, and Patricia A. Winters				8. Performing Organization Report No. L-11125	
9. Performing Organization Name and Address NASA Langley Research Center Hampton, VA 23665				10. Work Unit No. 506-25-31-01	
				11. Contract or Grant No.	
12. Sponsoring Agency Name and Address National Aeronautics and Space Administration Washington, DC 20546				13. Type of Report and Period Covered Technical Note	
				14. Sponsoring Agency Code	
15. Supplementary Notes Frank Hohl and Patricia A. Winters: Langley Research Center. S. Peter Gary: The College of William and Mary in Virginia, Williamsburg, Virginia.					
16. Abstract <p>Results are presented of a numerical integration of the three-dimensional relativistic equations of motion of electrons subject to given electric and magnetic fields deduced from experiments. Fields due to two different models are investigated. For the first model, the fields are those due to a circular distribution of axial current filaments. As the current filaments collapse toward the axis, large azimuthal magnetic and axial electric fields are induced. These fields effectively heat the electrons to a temperature of approximately 8 keV and accelerate electrons within the radius of the filaments to high axial velocities. Similar results are obtained for the current-reduction phase of focus formation. For the second model, the fields are those due to a uniform current distribution. Both the current-reduction and the compression phases were studied. There is little heating or acceleration of electrons during the compression phase because the electrons are tied to the magnetic field. However, during the current-reduction phase, electrons near the axis are accelerated toward the center electrode and reach energies of 100 keV. The computations are in general agreement with experimental results. A criterion is obtained which limits the runaway electron current to about 400 A. The criterion depends only on the electron temperature and thus is subject to experimental observation.</p>					
17. Key Words (Suggested by Author(s)) Plasma focus Electron heating			18. Distribution Statement Unclassified - Unlimited		
			Subject Category 75		
19. Security Classif. (of this report) Unclassified		20. Security Classif. (of this page) Unclassified		21. No. of Pages 35	22. Price* \$3.75

## ELECTRON DYNAMICS IN A PLASMA FOCUS

Frank Hohl, S. Peter Gary,\* and  
Patricia A. Winters  
Langley Research Center

### SUMMARY

Results are presented of a numerical integration of the three-dimensional relativistic equations of motion of electrons subject to given electric and magnetic fields deduced from experiments. Fields due to two different models are investigated. For the first model, the fields are those due to a circular distribution of axial current filaments. As the current filaments collapse toward the axis, large azimuthal magnetic and axial electric fields are induced. These fields effectively heat the electrons to a temperature of approximately 8 keV and accelerate electrons within the radius of the filaments to high axial velocities. Similar results are obtained for the current-reduction phase of focus formation. For the second model, the fields are those due to a uniform current distribution. Both the current-reduction and the compression phases were studied. There is little heating or acceleration of electrons during the compression phase because the electrons are tied to the magnetic field. However, during the current-reduction phase, electrons near the axis are accelerated toward the center electrode and reach energies of 100 keV. The computations are in general agreement with experimental results. A criterion is obtained which limits the runaway electron current to about 400 A. The criterion depends only on the electron temperature and thus is subject to experimental observation.

### INTRODUCTION

Plasma-focus devices have been extensively investigated in a number of laboratories. (See refs. 1 to 8.) Figure 1 illustrates the coaxial plasma-focus apparatus. The region of interest in the present investigation is the small cylindrical shaded region directly over the center electrode. This is the region where the dense, high-temperature plasma appears in the final stages of focus formation. Operation of the plasma focus with deuterium as the filling gas yields intense bursts of neutrons and X-rays. A two-dimensional fluid model of the plasma focus has been developed by Potter (ref. 9), and the model described well the initial phases of focus formation. However, such fluid models do not include the detailed processes of ion and electron heating occurring during the final phase of focus formation. To investigate the process of ion heating and acceleration in the plasma focus, a number of models have been used to determine ion trajectories in given fields deduced from experimental data. (See refs. 10 to 12.) Some of the more recent work on ion dynamics based on an improved model (refs. 13 and 14) is in good agreement with the experimental

---

\*The College of William and Mary in Virginia, Williamsburg, Virginia.

data. The purpose of the present paper is to present results on the electron acceleration in the plasma focus and to discuss the associated X-ray production.

X-ray emission from the plasma focus has been investigated by many different experimental groups. (See refs. 3, 4, and 15 to 19.) The experimental results show that the plasma focus emits a substantial flux of X-rays with energies greater than 100 keV. Also, the hard X-ray intensity is greatest in the direction pointing from the plasma to the anode, indicating that the X-rays are produced by high-energy electrons striking the anode (ref. 19).

Newman and Petrosian (ref. 20) have proposed a model of the plasma focus where electrons are accelerated during the current-sheet collapse (compression) phase, which would accelerate electrons away from the anode to produce X-rays in the plasma. However, this conclusion is not supported by experimental evidence. For example, figure 2 shows a picture from an X-ray pinhole camera of the plasma-focus formation process from the 50 kV 50 kJ plasma focus at the Langley Research Center. The usual pinhole camera picture shows only the X-ray emission from the electrode and from the very dense cone-shaped plasma directly above the center of the electrode. This result is caused by electrons accelerated downward and striking the electrode or the dense plasma. To determine the presence of any upward accelerated electrons, an aluminum plate was placed above the center electrode as shown in figure 2. No X-ray image of the aluminum target was observed, thus indicating that electrons are accelerated primarily downward toward the center electrode and not upward.

The uniform-current model used in the present paper shows that electrons are accelerated toward the center electrode in agreement with experimental results. The plasma-focus parameters used in the present paper are the same as those used in an earlier paper on ion heating in a plasma focus (ref. 14). That is, the peak current in the focus is taken to be 1 MA. During the collapse phase the collapse velocity is 180 km/s and the current-reduction phase results in a 30-percent decrease of the current in a time of 50 ns.

Two models of the current distribution are studied in the present paper. The first distribution is that due to a circular distribution of current filaments as observed by Bostick et al. (ref. 21). Evidence of such filaments has also been observed by radial tracks on the copper electrode from the plasma focus at the Langley Research Center. An example of such tracks is shown in figure 3. The central hole in the electrode is the result of energetic particle interaction resulting from focus formation. The second model investigated is a uniform current distribution used previously for the ion dynamics studies (refs. 13 and 14). For both models the collapse and the current-reduction phases are studied.

#### SYMBOLS

- $\vec{A}$  magnetic vector potential, webers/meter
- $\vec{B}$  magnetic field, teslas
- $c$  speed of light, meters/second

$\vec{E}$	electric field, volts/meter
$e$	magnitude of electronic charge, coulombs
$I$	current, amperes
$I_r$	runaway current, amperes
$\vec{j}$	current density, amperes/meter <sup>2</sup>
$m$	mass, kilograms
$m_e$	electron mass, kilograms
$m_i$	ion mass, kilograms
$n$	number of current filaments
$n_e$	electron-number density, meters <sup>-3</sup>
$R$	radius of current filaments or radius of current-carrying region, meters
$R_0$	initial radius of plasma column, meters
$r, \theta, z$	cylindrical coordinates
$\vec{r}$	position vector
$r_0$	radius of outer electrode, meters
$r_r$	runaway radius, meters
$T$	temperature derived from $\frac{1}{2} m \langle (v - \langle v \rangle)^2 \rangle$ , electronvolts
$T^*$	effective energy of electron beam derived from $\frac{1}{2} m \langle \langle v_z \rangle^2 \rangle$ , electronvolts
$t$	time, seconds
$V$	velocity
$\vec{V}$	velocity vector, meters/second
$V_{av}$	average drift velocity, meters/second
$V_c$	collapse velocity, 180 kilometers/second
$V_{th}$	thermal velocity, meters/second

$x, y, z$       rectangular coordinates  
 $\beta$             =  $\mu_0 n_e v_{av} / 2$   
 $\mu_0$             permeability of free space  
 $\tau$              time constant per second  
 $\Omega_c$           cyclotron frequency per second

Subscripts:

$e$              electron  
 $i$              ion  
 $\max$           maximum  
 $r, \theta, z$      r-,  $\theta$ -, and z-components  
 $x, y, z$       x-, y-, and z-components

Notation:

$\langle \rangle$           root-mean-square value  
 $\hat{\phantom{x}}$           unit vector

## THE MODEL

### Equations of Motion

The relativistic equations of motion for electrons subject to electric and magnetic fields are

$$\frac{d}{dt} \left( \frac{\vec{V}}{\sqrt{1 - \frac{v^2}{c^2}}} \right) = \frac{e}{m} (\vec{E} + \vec{V} \times \vec{B}) \quad (1)$$

and

$$\frac{d\vec{r}}{dt} = \vec{V}(t) \quad (2)$$

By neglecting the displacement current, the relevant Maxwell equations are

$$\nabla \times \vec{B} = \mu_0 \vec{J} \quad (3)$$

and

$$\nabla \times \vec{E} = - \frac{\partial \vec{B}}{\partial t} \quad (4)$$

In cylindrical coordinates with the current in the z-direction, the fields are

$$\vec{B} = \hat{\theta} B_{\theta} + \hat{r} B_r \quad (5)$$

and

$$\vec{E} = \hat{z} E_z \quad (6)$$

Equations (1) and (2) are integrated numerically by using the time-centered leap-frog method.

#### Current Filament

The vector potential for a ring of current filaments in the plasma focus is approximated by the vector potential for an isolated ring of  $n$  current filaments equally spaced around a circle of radius  $R$ . That is,

$$A_z(r, \theta) = - \frac{\mu_0 I}{4\pi} \ln (R^{2n} - 2R^n r^n \cos n\theta + r^{2n}) + C \quad (7)$$

where  $I$  is the current in each filament and  $C$  is a constant. The magnetic field is obtained from  $\vec{B} = \nabla \times \vec{A}$ , or

$$B_{\theta} = - \frac{\partial A_z}{\partial r} = - \frac{\mu_0 n I}{2\pi r} \frac{\left(\frac{r}{R}\right)^n \cos n\theta - \left(\frac{r}{R}\right)^{2n}}{1 - 2\left(\frac{r}{R}\right)^n \cos n\theta + \left(\frac{r}{R}\right)^{2n}} \quad (8)$$

and

$$B_r = \frac{1}{r} \frac{\partial A_z}{\partial \theta} = - \frac{\mu_0 n I}{2\pi r} \frac{\left(\frac{r}{R}\right)^n \sin n\theta}{1 - 2\left(\frac{r}{R}\right)^n \cos n\theta + \left(\frac{r}{R}\right)^{2n}} \quad (9)$$

The magnitude of  $B$  is

$$B = \sqrt{B_{\theta}^2 + B_r^2} = \frac{\mu_0 n I}{2\pi r} \frac{\left(\frac{r}{R}\right)^n}{\left[1 - 2\left(\frac{r}{R}\right)^n \cos n\theta + \left(\frac{r}{R}\right)^{2n}\right]^{1/2}} \quad (10)$$

For the parameters  $n = 10$ ,  $R = 10^{-3}$  m, and  $nI = 10^6$  A, the constant  $B$  contours are shown in figure 4. There are large gradients of  $B$  near the

filaments and  $B$  is essentially zero in the region interior to the ring of filaments. This behavior is again displayed in figure 5 which shows  $B$  as a function of  $r$ . The electric field induced by the changing current and resultant magnetic field is obtained from

$$E_z = - \frac{\partial A_z}{\partial t} \quad (11)$$

During the compression phase the radius  $R$  of the current filaments is taken to collapse with the experimentally determined velocity  $V_c = -dR/dt$  of 180 km/s. (See refs. 4 and 14.) Thus, the induced electric field during the compression phase is

$$E_z = V_c \frac{\mu_0 n I}{2\pi R} \frac{1 - \left(\frac{r}{R}\right)^n \cos n\theta}{1 - 2\left(\frac{r}{R}\right)^n \cos n\theta + \left(\frac{r}{R}\right)^{2n}} \quad (12)$$

Note that for  $r = r_o$  (where  $r_o = 0.05$  m, the radius of the outer electrode),  $E_z$  is essentially zero and no term need be added to equation (12) to satisfy the boundary condition  $E_z(r_o) = 0$ . Figure 6 shows the radial variation of the induced field at various angles between two filaments. Note that the angle between filaments is  $36^\circ$  and the angles  $0^\circ$  and  $36^\circ$  pass through the center of filaments.

During the current-reduction phase,  $R$  remains constant and the electric current  $I$  varies as

$$I = I_0(1 - \tau t) \quad (13)$$

where  $I_0 = I$  ( $t = 0$ ) and where  $\tau$  is determined in agreement with experimental results to obtain a 30-percent current reduction in 50 ns. Thus, the axial electric field during the current-reduction phase is

$$E_z = - \frac{\mu_0 I_0 \tau}{4\pi} \left[ \ln \left( R^{2n} - 2R^n r^n \cos n\theta + r^{2n} \right) - \ln \left( R^{2n} - 2R^n r_o \cos n\theta + r_o^{2n} \right) \right] \quad (14)$$

The second term in the equation is a constant such that the induced electric field becomes zero at radius  $r_o$  which is the radius of the outer electrode. Figure 7 shows the radial variation of the induced axial field during the current-reduction phase as given by equation (14). Note that the 50-ns current-reduction phase is probably too long. Thus, the induced field in the central region during the current-reduction phase is expected to be about the same magnitude as the peak field during the compression phase as shown in figure 6.

#### Uniform Current

The magnetic and electric fields for the uniform-current density model used in the present report are the same as those used previously in reference 14, and

their derivation will not be repeated here. During the compression phase the magnetic field is

$$B_{\theta}(r,t) = \frac{\mu_0 I}{2\pi R^2} r \quad (r \leq R(t))$$

$$B_{\theta}(r,t) = \frac{\mu_0 I}{2\pi r} \quad (r > R(t))$$

where  $R(t)$  is now the radius of the current-carrying region and  $I$  is the total current. The corresponding induced electric field is

$$E_z(r,t) = \frac{\mu_0 I V_c}{2\pi R^3} (r^2 - R^2(t)) \quad (r \leq R(t))$$

$$E_z(r,t) = 0 \quad (r > R(t))$$

For the current-reduction phase the magnetic field is

$$B_{\theta}(r,t) = \frac{\mu_0 I_0}{2\pi R^2} r(1 - \tau t) \quad (r \leq R(t))$$

$$B_{\theta}(r,t) = \frac{\mu_0 I_0}{2\pi r} (1 - \tau t) \quad (R(t) < r < r_0)$$

resulting in an induced electric field given by

$$E_z(r) = - \frac{\mu_0 I_0 \tau}{4\pi R^2} \left( r^2 - 2R^2 \ln \frac{r_0}{R} \right) \quad (r \leq R)$$

$$E_z(r) = - \frac{\mu_0 I_0 \tau}{4\pi} \left( 1 + 2 \ln \frac{r}{R} - 2 \ln \frac{r_0}{R} \right) \quad (R < r < r_0)$$

## RESULTS AND ANALYSIS

### Current-Filament Model

Filamentary current structure has been observed during the collapse or compression phase of focus formation. It, therefore, seems appropriate to investigate the effect of the associated fields on the plasma electrons. Details of the fields are shown in figures 4 to 7. Figure 8 shows the evolution of the electron distribution represented by 3000 electrons during the compression phase. The initial conditions of the electrons are generated by a pseudo random-number generator. The initial velocities were given a Gaussian distribution, whereas the initial positions were given a uniform distribution. The magnetic and induced electric fields acting on the electrons are given by equations (8), (9), and (10). The variable  $R$  defining the radial position of the current filaments is given by

$$R(t) = R_0 - V_0 t$$

Experimental results (ref. 4) indicate that the aforementioned expression is valid for  $0 \leq t \leq 50$  ns. However, because of the rapid electron response to the strong induced electric fields, the calculations are performed for only a fraction of a ns. Note that electrons are expelled from the regions of high magnetic field near the filaments. Also, electrons concentrate in magnetic wells between filaments and in the central region. The evolution of the total electron velocity as a function of radius is given in figure 9. As can be seen from figures 5 and 6, the magnetic field is essentially zero in the region interior to the ring of filaments, whereas the axial electric field is large in this region. Thus, the electrons in the central region quickly reach large axial velocities and essentially free stream under the influence of the induced axial electric field. As the electrons reach an axial distance of 1.5 cm from their initial  $z = 0$  position, they are assumed to have escaped the focus region and are taken out of the calculations. This explains the absence of accelerated electrons in the central regions after  $t = 0.15$  ns in figure 9. Figure 10 displays the energy of the electrons during the compression phase. The symbol  $T^*$  denotes the energy associated with the axial motion, whereas  $T_{xy}$  is an effective transverse temperature. Note that the electrons are quickly heated to about 8 keV.

Similar results are obtained during the current-reduction phase. As shown in figure 7, the axial field is now in the opposite direction and accelerates electrons toward the center electrode. Figure 11 shows the evolution of the electron distribution. The evolution of the electron velocities is shown in figure 12.

The large central region of near-zero magnetic field for the filament model allows electron acceleration away from the anode during the compression phase and toward the anode during the current-reduction phase. Electron acceleration away from the anode as obtained with the filament model is not supported by experimental data. The model does explain the experimentally observed electron heating. The large number of electrons accelerated to relativistic velocities in the region interior to the ring of filaments would give rise to strong magnetic fields. These fields would impede the electrons and lead to a reduction in the current. Therefore, a self-consistent computation seems necessary for accurate modeling.

#### Uniform-Current Model

The uniform-current model (ref. 14) is probably the simplest model one can assume for the plasma focus. Since, in this case, the magnetic field increases linearly with  $r$ , the region of  $B \approx 0$  available to produce runaway electrons is much smaller than that in the filament model. Thus, the results are much less likely to be in conflict with a self-consistent computation. Figure 13 demonstrates the evolution of the x-y positions of 3000 electrons with an initially uniform distribution during the compression phase. The direction of the  $\vec{E} \times \vec{B}$  drift is away from the axis, so that the electrons leave a "hole" on the axis. Particles are most likely to be accelerated near the axis where  $B$  is small; but since the induced electric field during the collapse phase drives electrons

away from this region, very little acceleration takes place. There is essentially no heating of the electrons because of trapping by the strong magnetic field. The inclusion of collisions would not affect these results appreciably since there are at least  $10^4$  cyclotron periods per collision time. Figure 14 shows the time evolution of the axial velocity as a function of radial position during the compression phase. As can be seen, only a few electrons are heated to moderate temperatures near the central region.

The evolution of the x-y distribution of electrons for the current-reduction phase is shown in figure 15. During this phase the  $\vec{E} \times \vec{B}$  drift forces electrons toward the axis. The corresponding evolution of the electron velocities as a function of radius is shown in figure 16. Away from the central region electrons are effectively tied to the magnetic field and little heating or acceleration takes place. However, as electrons forced by the  $\vec{E} \times \vec{B}$  drift approach within a Larmor radius of the axis they are free to accelerate under the strong  $eE_z$  force. These electrons quickly gain kinetic energy in the direction opposite to  $J_z$ . Figures 17 and 18 show two examples of such electron trajectories as they approach the axis and are then accelerated in the z-direction toward the center electrode. At a large radius  $r$ , these trajectories are well described by the drift approximation

$$\vec{v} = \frac{\vec{E}(r) \times \vec{B}(r)}{B^2(r)}$$

However, as the electron approaches within a Larmor radius of the axis, it "runs away," although its angular momentum requires it to keep circling the axis as it accelerates. The time-averaged energy distribution of the runaway electrons is found to be inversely proportional to the electron energy.

Figure 19 shows a comparison of the X-ray emission experimentally determined from the 25 kJ 20 kV plasma focus at the Langley Research Center with the emission obtained from the "runaway" electrons impinging on the center electrode. The X-ray pattern is determined from the electron velocity vectors by using the thick target approximation; that is, the emitted energy is uniformly distributed in frequency up to the energy of the incident electron. For the low-energy emission there is good agreement; whereas, because of insufficient experimental data, the agreement is questionable for the high-energy emission.

#### Runaway-Current Limitation

In this section the uniform-current model is used to predict some properties of the runaway electrons that may be subject to experimental observation. For a uniform-current distribution,

$$B_\theta(r) = \beta r$$

$$\beta = \frac{\mu_0}{2} en_e V_{av}$$

where  $V_{av}$  is the average drift of the species within radius  $r$  and the plasma density  $n_e$  is assumed constant. Particles with Larmor radius greater than

their radial position are free to run away. Since the Larmor radius decreases with radial position, all particles within a radius  $r_r$ , determined by setting the radial position equal to the Larmor radius, are free to run away. That is,

$$r_r = \frac{V_{th}}{\Omega_c} = \frac{V_{th}m}{e\beta r_r}$$

where  $V_{th} = (T/m)^{1/2}$ , the average particle thermal velocity, and  $\Omega_c$  is the cyclotron frequency. Simplified, the runaway radius becomes

$$r_r = \left( \frac{\sqrt{Tm}}{e\beta} \right)^{1/2} \quad (15)$$

If  $T_e = T_i$ , the number of runaway electrons will be  $(m_e/m_i)^{1/2}$  times the number of runaway ions (ref. 13). However, since the ion response time is much larger than that of the electrons, ion runaway current would be important only on a much larger time scale than that investigated here. For typical focus parameters ( $T = 1$  keV;  $\beta = 2 \times 10^5$  T/m), the electron  $r_r$  is approximately equal to  $10^{-5}$  m (see figs. 17 and 18) which is quite small compared to the radius of the focus plasma. However, after runaway of electrons occurs within  $r_r$ ,  $\beta$

could possibly reach values as high as  $3 \times 10^8$  T/m (e.g., for  $n = 10^{25}$  m<sup>-3</sup> and  $V_{av} \approx c$ ) resulting in a minimum value for  $r_r$  of approximately  $10^{-6}$  m.

Further, equation (15) can be used to estimate the total current carried by runaway particles:

$$I_r = neV_{av}\pi r_r^2 = \frac{2\pi}{\mu_0 e} \sqrt{Tm} \quad (16)$$

This is a remarkable result because it depends upon only a simple experimental parameter, the species temperature. For a typical  $T_e = 1$  keV,  $I_r \approx 400$  A which is, of course, very small compared to the total current of approximately 1 MA discharged through a focus.

The derivation of equation (16) is similar, but not equivalent, to a simple derivation of the well-known Alfvén-Lawson criterion for the maximum current which can be carried by a charge-neutralized, relativistic electron beam (ref. 22). In both cases the argument hinges on equating the electron Larmor radius to the volume containing the high-speed electrons. The important difference is that, in the relativistic-beam case, this velocity is taken as the drift speed of the beam  $V_{av}$ ; whereas in the plasma focus, the electron thermal velocity  $V_{th}$  is the appropriate quantity and  $V_{av}$  drops out of the final expression for  $I_r$ .

## DISCUSSION

Although the computations presented for the filament and uniform-current models are not self-consistent, equation (16) is a self-consistent result within the assumption of uniform current. That is, if the electron current density (for some reason) increases,  $\beta$  also increases and  $r_r$  decreases. Thus, fewer

electrons are free to run away and the effects of increasing  $\vec{J}$  and decreasing runaway radius compensate each other so that  $I_r$  remains constant.

It is important to note that, because the present model assumes that the electric and magnetic fields are given, it cannot predict the energy distribution of the runaway electrons nor the duration of the associated X-ray pulse. Therefore, it is difficult at present to make quantitative comparisons with experimental results. These results are usually given as total runaway electron energy inferred from measurements of the hard X-ray energy emitted by the focus.

Harries et al. (ref. 19) have observed X-rays above 50 keV emitted for 100 ns and have determined an electron-beam energy of about 1 J. By assuming an average electron energy of about 50 keV, they have estimated an average current of 200 A, in approximate agreement with the present prediction. However, Gullickson and Barlett (ref. 18) infer a total energy of 1 kJ for electrons with energies greater than about 100 keV in 10 ns, and Maisonnier et al. (ref. 23) estimate 600 J for 100 keV electrons. Since these latter results imply runaway-current orders of magnitude larger than the present prediction, further work, both experimental and theoretical, would be desirable to resolve this discrepancy.

In spite of these limitations, the present model does make an unambiguous prediction which is subject to direct experimental verification: that is, runaway electrons must be accelerated toward the anode. The reason for this, as first discussed in reference 13, and as indicated here, is that axial electric fields pointing against the current flow cause charged particles to drift toward larger radii, away from the runaway region near the axes; whereas  $\vec{E}$  parallel to  $\vec{J}$  "pinches" electrons and ions toward the  $B = 0$  region where runaway can occur.

This prediction implies that ions are accelerated away from the anode, an often-demonstrated experimental result, and that electrons run away toward the anode. Recent X-ray data (refs. 18 and 19; also, fig. 2) have given strong support to this prediction for the electrons. The present prediction is directly opposed to that of Newman and Petrosian (ref. 20) who claim that electrons are accelerated away from the anode.

The present work suggests that the X-ray emitting, axially oriented, filament-like structures observed by Bostick et al. (ref. 16) are narrow channels of high-speed electrons accelerated by electric fields induced during the current-reduction phase of the focus. The smallness of  $r_r$  does not preclude the simultaneous existence of more than one of these channels, as suggested by Bostick, but the present theory is not yet adequate to predict the conditions necessary for the development of multiple filamentation.

Equations (15) and (16) may have relevance to ions as well, but these equations should be applied with care since  $r_r$  for ions can be of the same order of magnitude as the plasma radius, and the uniform-current approximation is probably not valid over the whole cross section of the focus. Thus, equation (16) suggests, rather than predicts, that runaway ions can carry substantially more current and energy than runaway electrons and that the focus may be a good device for accelerating very heavy ions.

## CONCLUDING REMARKS

Results are presented of a numerical integration of the three-dimensional relativistic equations of motion of electrons subject to given electric and magnetic fields deduced from experiments. Fields due to two different models are investigated. For the first model, the fields are those due to a circular distribution of axial current filaments. As the current filaments collapse toward the axis, large azimuthal magnetic and axial electric fields are induced. These fields effectively heat the electrons to a temperature of approximately 8 keV and accelerate electrons within the radius of the filaments to high axial velocities. Similar results are obtained for the current-reduction phase of focus formation. For the second model, the fields are those due to a uniform current distribution. Both the current-reduction and the compression phases were studied. There is little heating or acceleration of electrons during the compression phase because the electrons are tied to the magnetic field. However, during the current-reduction phase, electrons near the axis are accelerated toward the center electrode and reach energies of 100 keV. The computations are in general agreement with experimental results. A criterion is obtained which limits the runaway electron current to about 400 A. The criterion depends only on the electron temperature and thus is subject to experimental observation.

Langley Research Center  
National Aeronautics and Space Administration  
Hampton, VA 23665  
December 15, 1976

## REFERENCES

1. Mather, J. W.: Dense Plasma Focus. Plasma Physics. Vol. 9, Pt. B of Methods of Experimental Physics, Ralph H. Lovberg and Hans R. Griem, eds., Academic Press, Inc., 1971, pp. 187-249.
2. Mather, Joseph W.; and Bottoms, Paul J.: Characteristics of the Dense Plasma Focus Discharge. Phys. Fluids, vol. 11, no. 3, Mar. 1968, pp. 611-618.
3. Lee, J. H.; Loebbaka, D. S.; and Roos, C. E.: Hard X-Ray Spectrum of a Plasma Focus. Plasma Phys., vol. 13, no. 4, Apr. 1971, pp. 347-349.
4. Jalufka, Nelson W.; and Lee, Ja H.: Current Sheet Collapse in a Plasma Focus. Phys. Fluids, vol. 15, no. 11, Nov. 1972, pp. 1954-1958.
5. Gratreau, P.; Luzzi, G.; Maisonnier, Ch.; Pecorella, F.; Rager, J. P.; Robouch, B. V.; and Samuelli, M.: Structure of the Dense Plasma Focus, Part I: Numerical Calculations, X-Ray and Optical Measurements. Plasma Physics and Controlled Nuclear Fusion Research - 1971, Vol. I, Int. At. Energy Agency, 1971, pp. 511-521.
6. Peacock, N. J.; Hobby, M. G.; and Morgan, P. D.: Measurements of the Plasma Confinement and Ion Energy in the Dense Plasma Focus. Plasma Physics and Controlled Nuclear Fusion Research - 1971, Vol. I, Int. At. Energy Agency, 1971, pp. 537-551.
7. Bernard, A.; Cesari, G.; Coudeville, A.; Jolas, A.; de Mascureau, J.; and Watteau, J. P.: Etude du Plasma Focus par Diffusion Thomson et Anisotropie des Neutrons Pendant l'Emission Neutronique. Plasma Physics and Controlled Nuclear Fusion Research - 1971, Volume I, Int. At. Energy Agency, 1971, pp. 553-560.
8. Mather, J. W.; Bottoms, P. J.; Carpenter, J. P.; Ware, K. D.; and Williams, A. H.: Recent Studies of Dense Plasma Focus. Plasma Physics and Controlled Nuclear Fusion Research - 1971, Volume I, Int. At. Energy Agency, 1971, pp. 561-570.
9. Potter, D. E.: Numerical Studies of the Plasma Focus. Phys. Fluids, vol. 14, no. 9, Sept. 1971, pp. 1911-1924.
10. Bernstein, Melvin J.: Deuteron Acceleration and Neutron Production in Pinch Discharges. Phys. Rev. Lett., vol. 24, no. 13, Mar. 30, 1970, pp. 724-727.
11. Bernstein, Melvin J.: Acceleration Mechanism for Neutron Production in Plasma Focus and z-Pinch Discharges. Phys. Fluids, vol. 13, no. 11, Nov. 1970, pp. 2858-2866.
12. Bernstein, M. J.; and Comisar, G. G.: Neutron Energy and Flux Distributions From a Crossed-Field Acceleration Model of Plasma Focus and z-Pinch Discharges. Phys. Fluids, vol. 15, no. 4, Apr. 1972, pp. 700-707.

13. Gary, S. Peter; and Hohl, Frank: Ion Kinematics in a Plasma Focus. Phys. Fluids, vol. 16, no. 7, July 1973, pp. 997-1002.
14. Hohl, Frank; and Gary, S. Peter: Ion Heating in a Plasma Focus. NASA TN D-7765, 1974.
15. Van Paassen, H. L. L.; Vandre, R. H.; and White, R. Stephen: X-Ray Spectra From Dense Plasma Focus Devices. Phys. Fluids, vol. 13, no. 10, Oct. 1970, pp. 2606-2612.
16. Bostick, W. H.; Nardi, V.; and Prior, W.: X-Ray Fine Structure of Dense Plasma in a Co-Axial Accelerator. Plasma Phys., vol. 8, pt. 1, Aug. 1972, pp. 7-20.
17. Belyaeva, I. F.; and Filippov, N. V.: Location of Fast Deuterons in a Plasma Focus. Nucl. Fusion, vol. 13, no. 6, Dec. 1973, pp. 881-882.
18. Gullickson, R. L.; and Barlett, R. H.: X-Ray Analysis for Electron Beam Enhancement in the Plasma Focus Device. Advances in X-Ray Analysis, Volume 18, William L. Pickles, Charles S. Barrett, John B. Newkirk, and Clayton O. Ruud, eds., Plenum Press, c.1975, pp. 184-196.
19. Harries, W. L.; Lee, J. H.; and McFarland, D. R.: Trajectories of High-Energy Electrons in a Plasma Focus. Bull. American Phys. Soc., ser. II, vol. 20, no. 10, Oct. 1975, p. 1370.
20. Newman, C. E.; and Petrosian, Vahé: Production of Hard X Rays in a Plasma Focus. Phys. Fluids, vol. 18, no. 5, May 1975, pp. 547-551.
21. Bostick, W. H.; Nardi, V.; Grunberger, L.; and Prior, W.: Observation of Solar Flare Type Processes in the Laboratory. Solar Magnetic Fields, Robert Howard, ed., D. Reidel Pub. Co. (Dordrecht, Holland), 1971, pp. 512-525.
22. Hammer, D. A.; and Rostoker, N.: Propagation of High Current Relativistic Electron Beams. Phys. Fluids, vol. 13, no. 7, July 1970, pp. 1831-1850.
23. Maisonnier, Ch.; Pecorella, F.; Rager, J. P.; Samuelli, M.; Strangio, C.; and Messina, A.: Comparative Studies of Plasma Focus Devices. IAEA-33/E6-2, Fifth Conference on Plasma Physics and Controlled Nuclear Fusion Research (Tokyo, Japan), Nov. 1975.

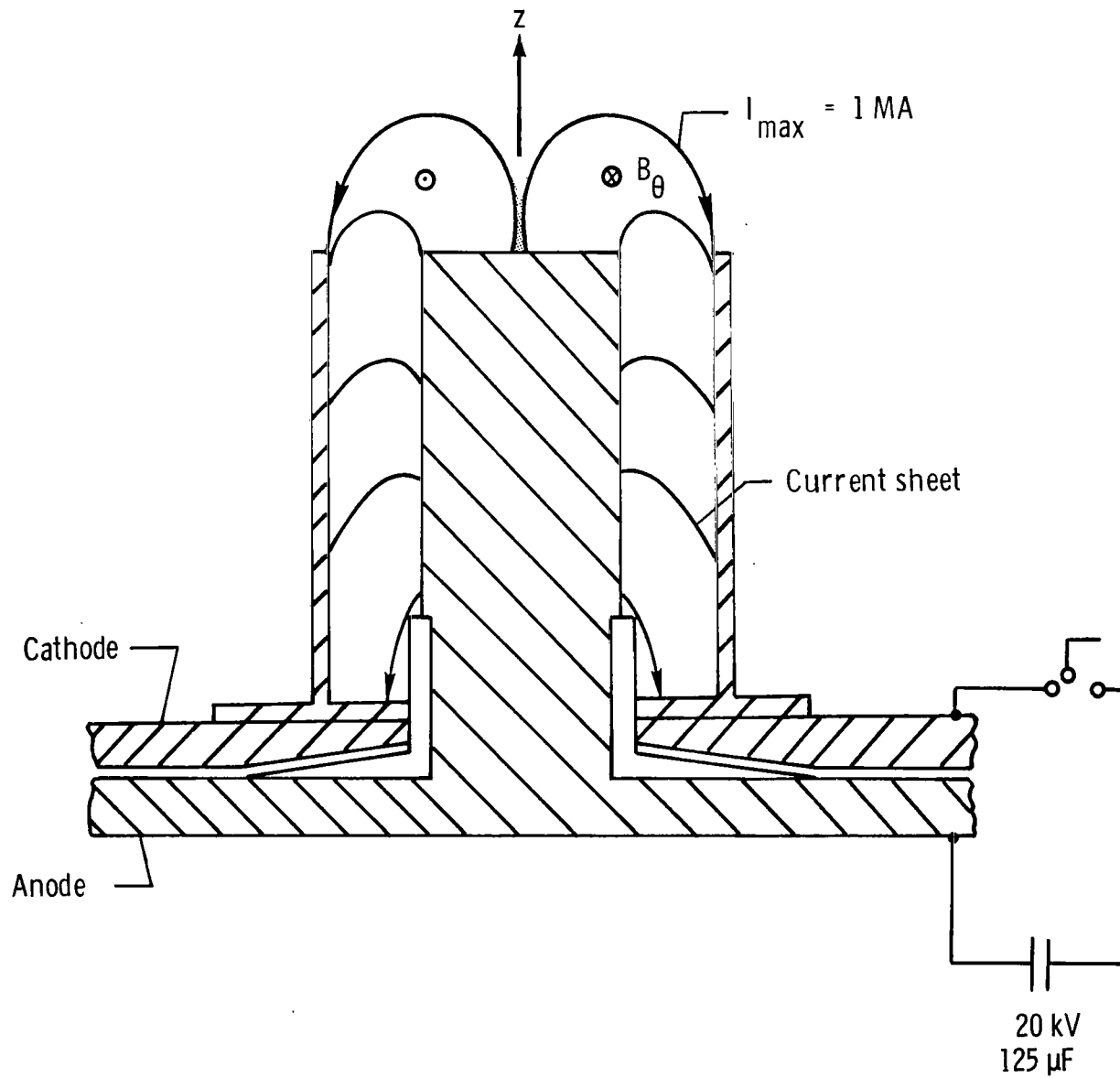
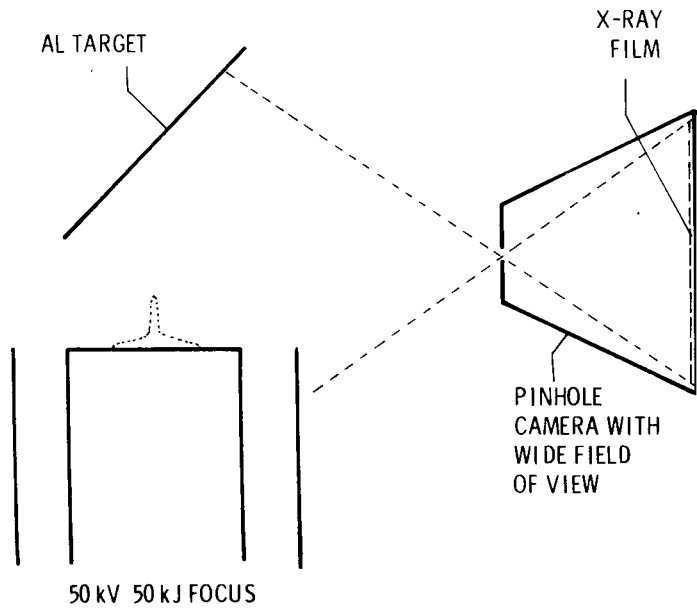
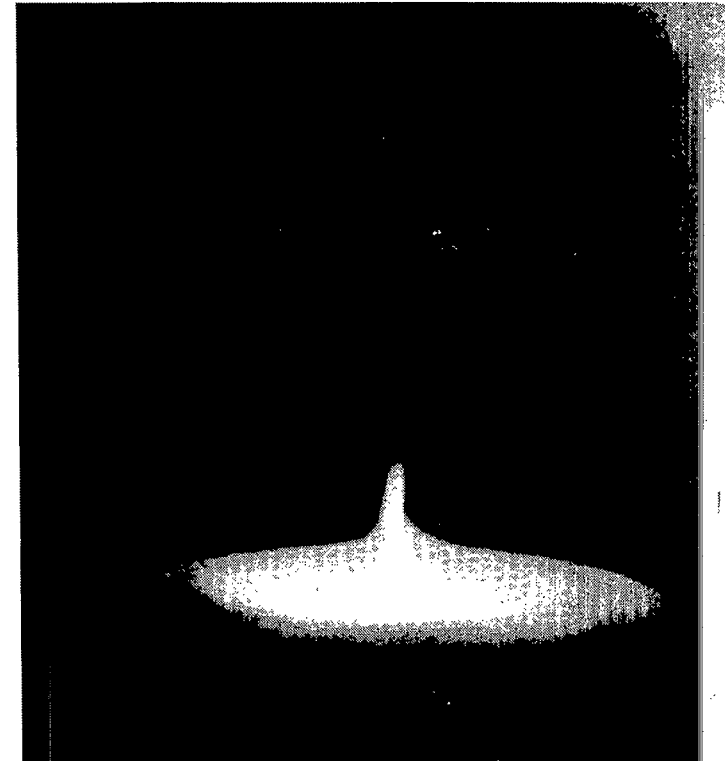


Figure 1.- Cross-sectional view through coaxial plasma-focus apparatus.



(a) Experimental setup.



(b) X-ray photograph.

L-76-7516

Figure 2.- Experimental setup to determine direction of electron acceleration in the plasma focus. No X-rays are observed from the aluminum target, indicating that electrons are accelerated downward toward the center electrode from which strong X-ray emission is observed.

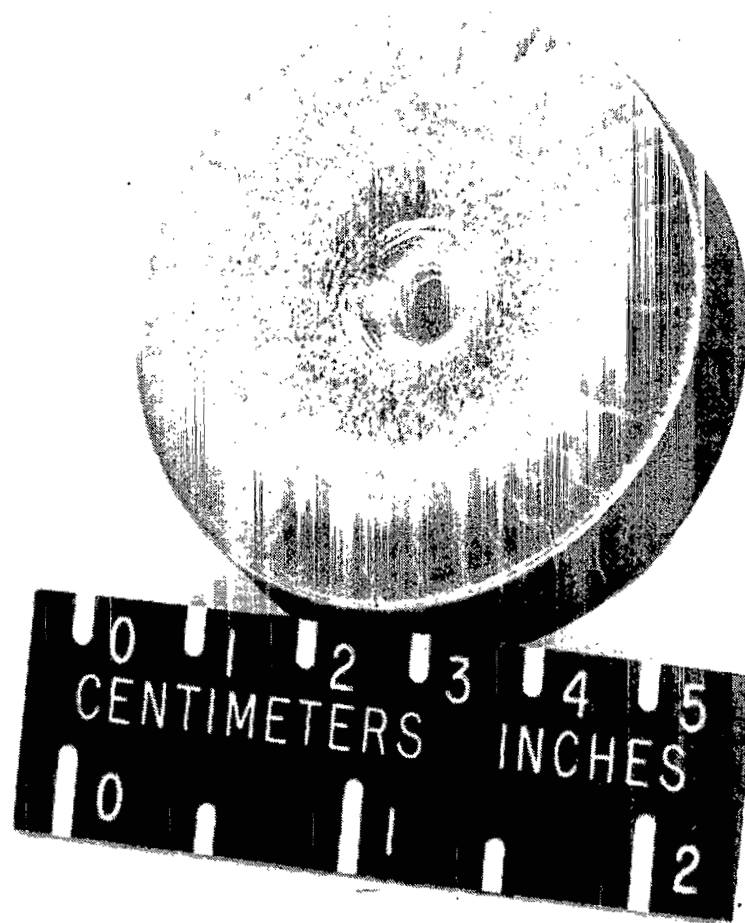


Figure 3.- Center electrode from the coaxial plasma focus showing radial tracks produced by current filaments.

L-73-2931

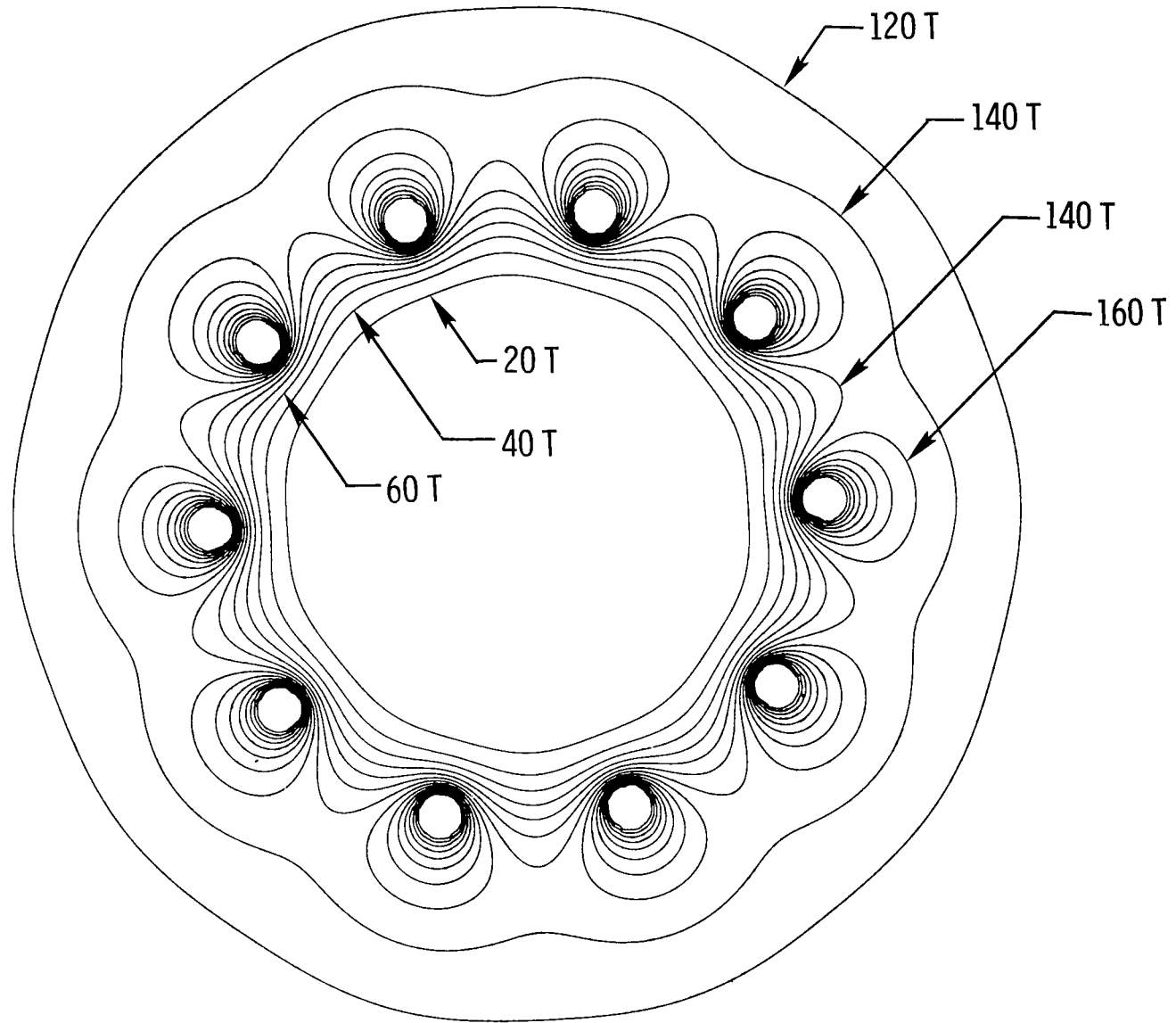


Figure 4.- Contours of constant  $B$  for 10 current filaments uniformly distributed around a circle with a diameter of 2 mm. Each filament carries 100 kA resulting in a total current of 1 MA.

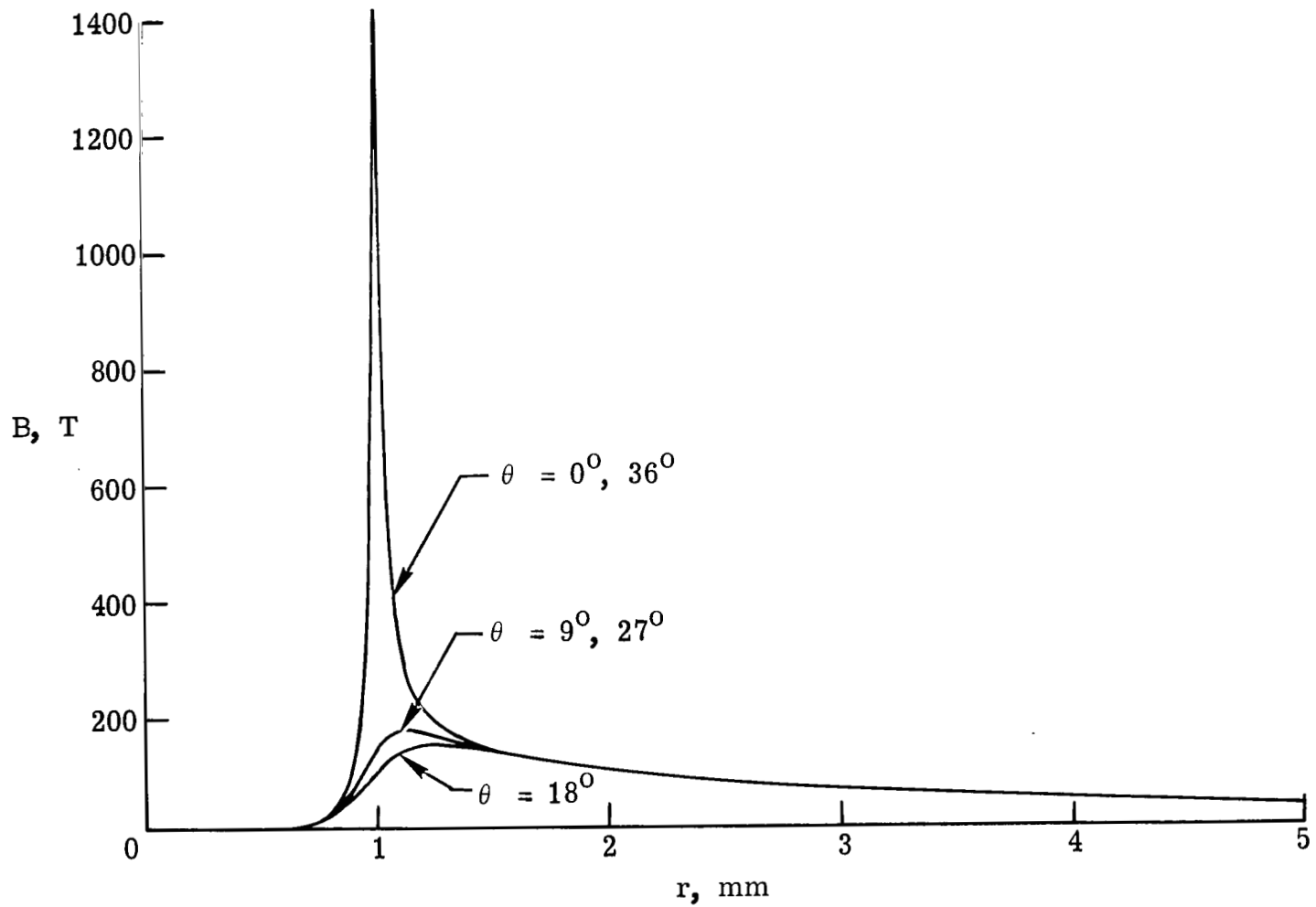


Figure 5.- Radial variation of  $B$  at various angles. Note that  $B$  is essentially zero in the central region inside the ring of filaments.

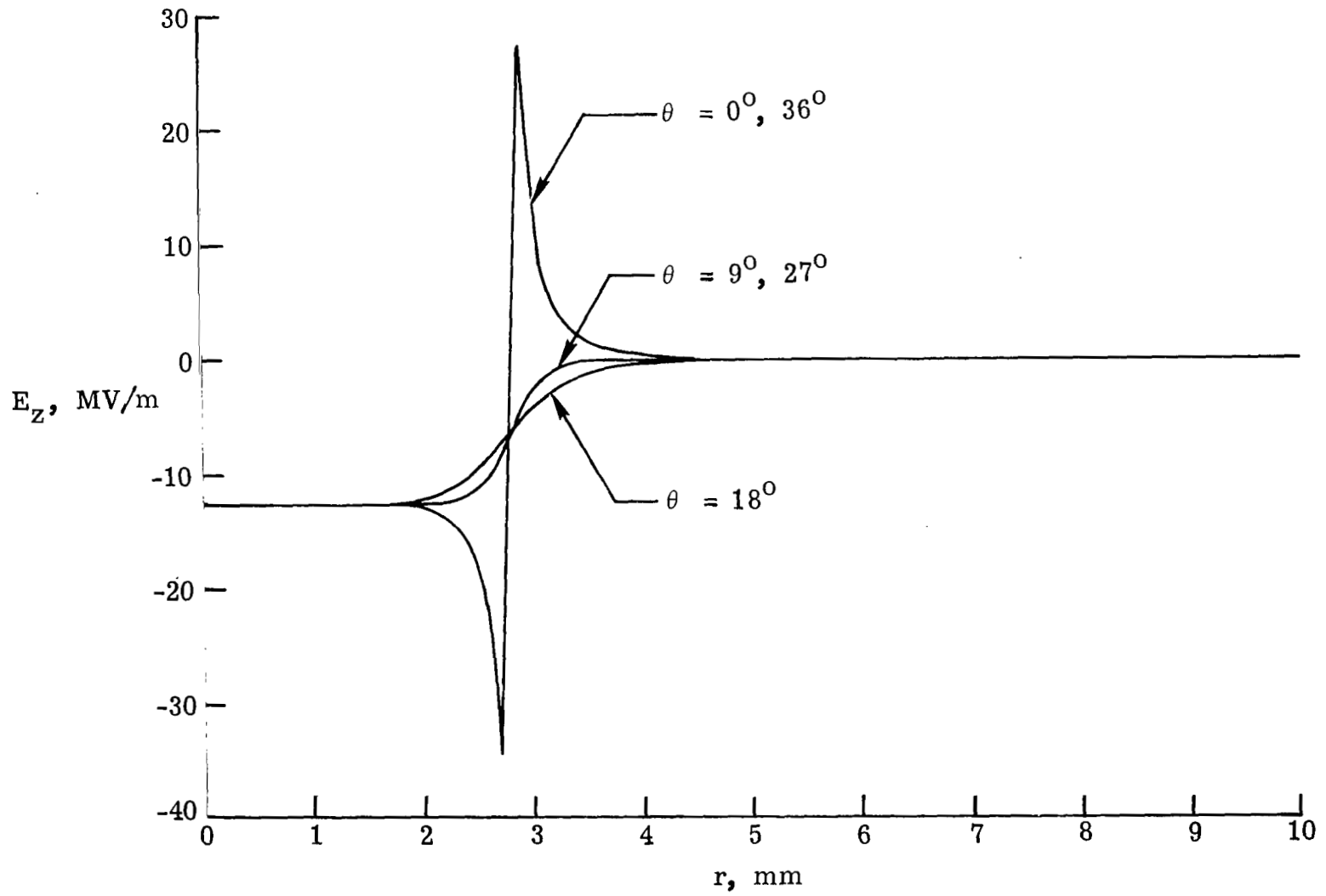


Figure 6.- Induced axial electric field during the compression for the filament model.

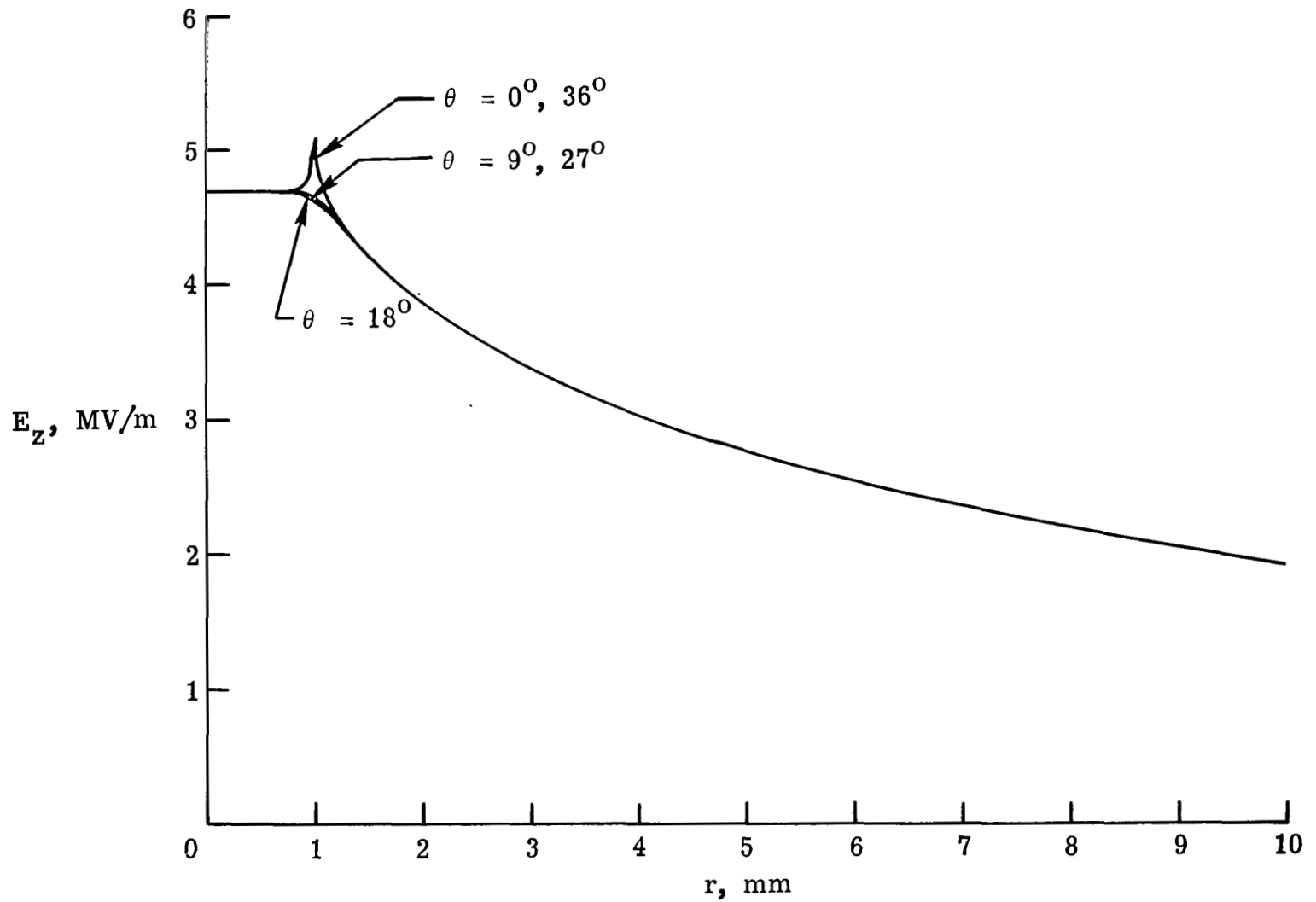


Figure 7.- Induced axial electric field in the filament model during the current reduction phase.  
 Note that the positive field accelerates electrons toward the anode.

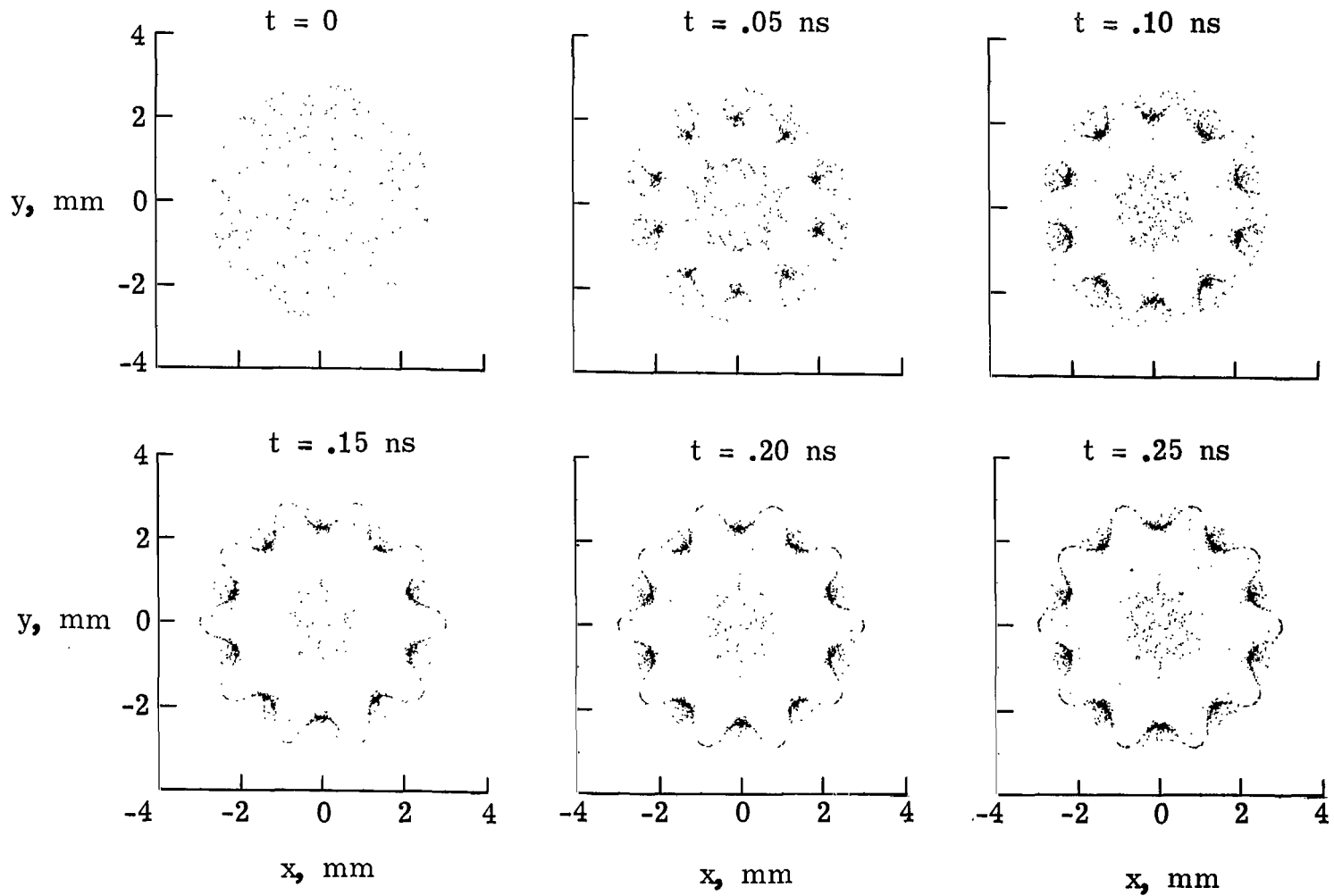


Figure 8.- Evolution of the x-y distribution of 3000 electrons during compression phase for the 10-filament model. Electrons are trapped and heated near and outside the filament radius, whereas electrons in the central region are accelerated upward away from the center electrode.

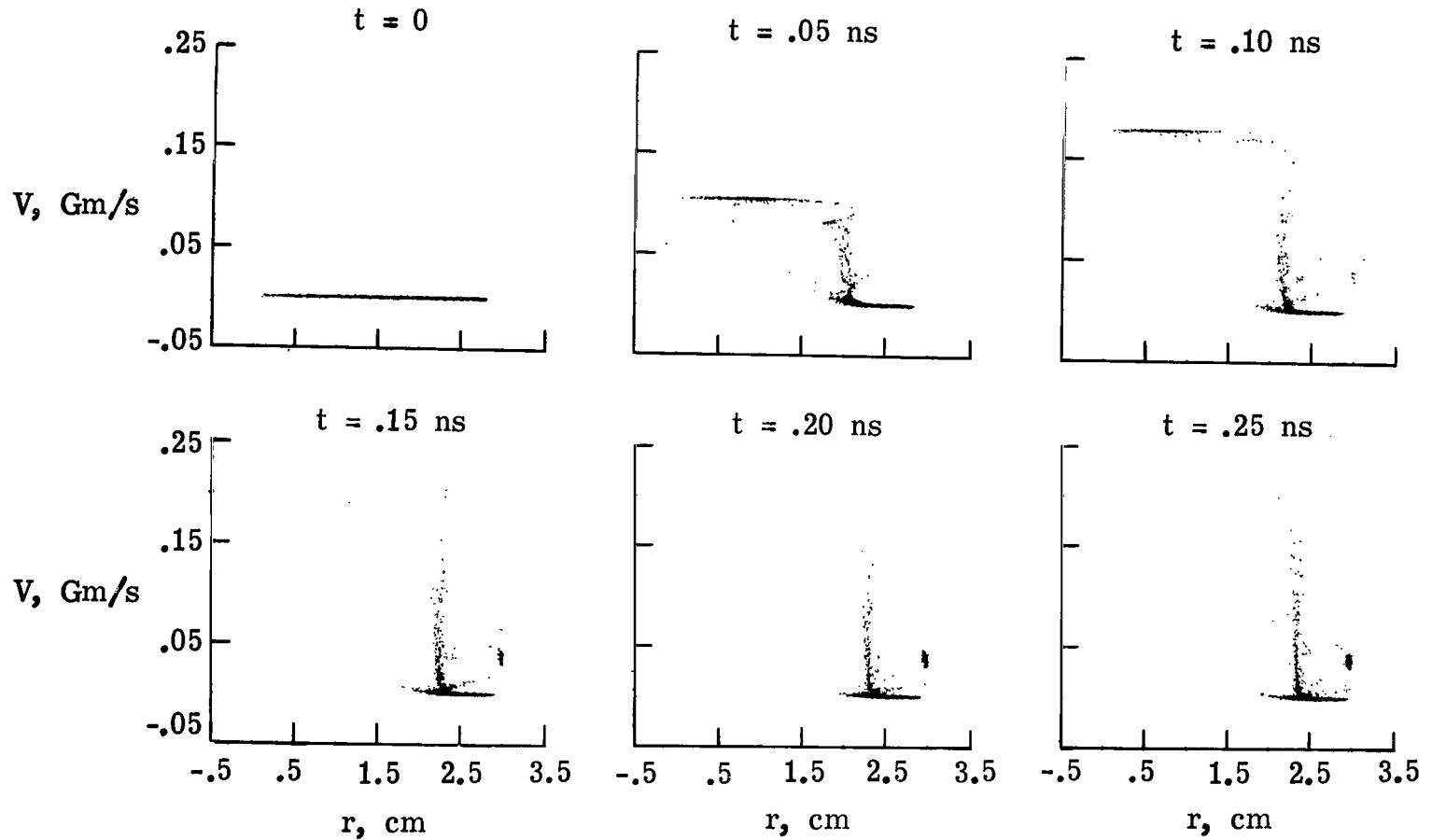


Figure 9.- Evolution of the distribution of 3000 electrons in V-r space during the compression phase. As electrons reach a distance of 1.5 cm from their initial  $z = 0$  axial position, they are removed from the calculation.

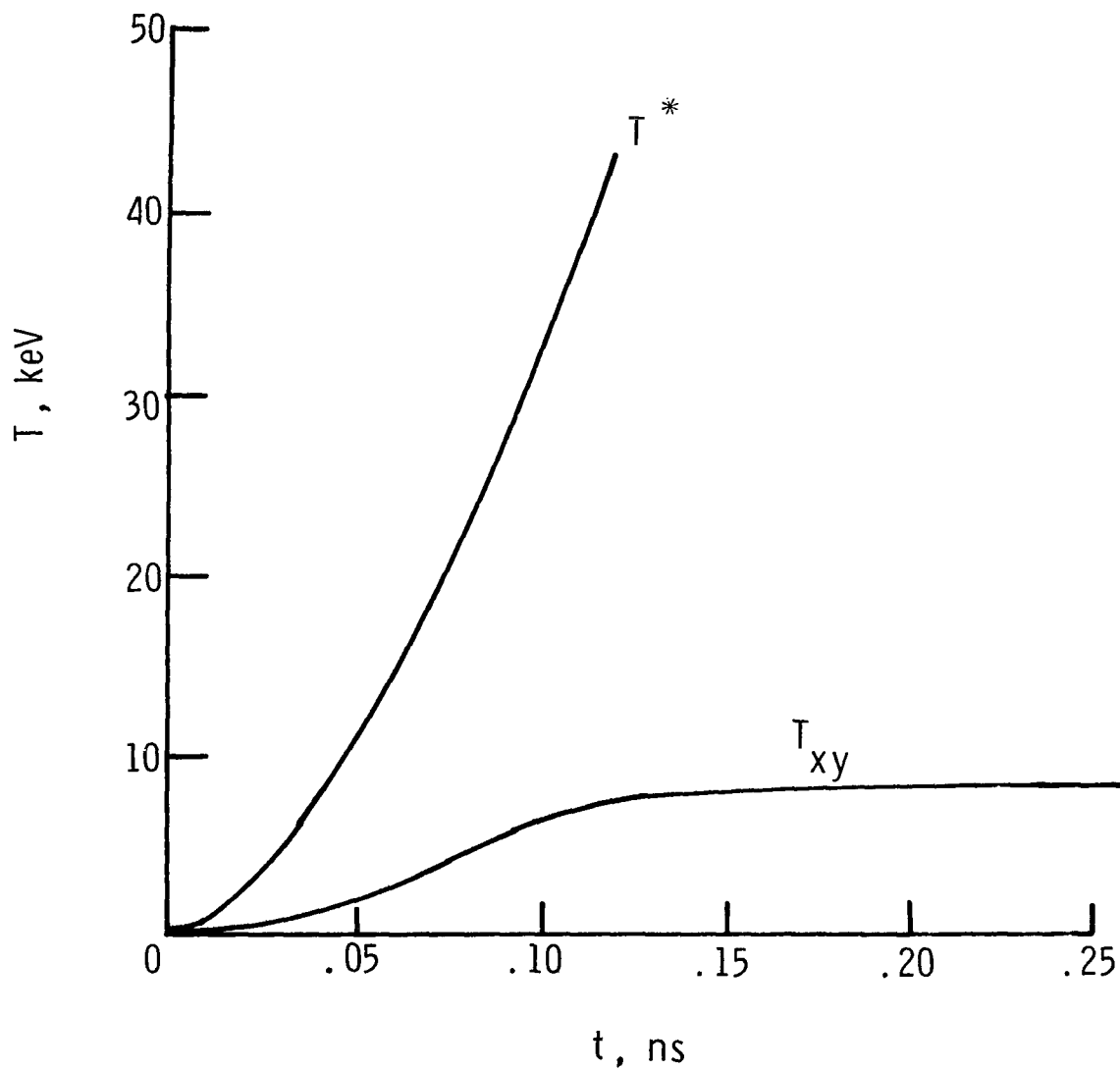


Figure 10.- Time variation of transverse temperature  $T_{xy}$  and z-directed beam energy  $T^*$  of electrons during the compression phase in the current filament model.

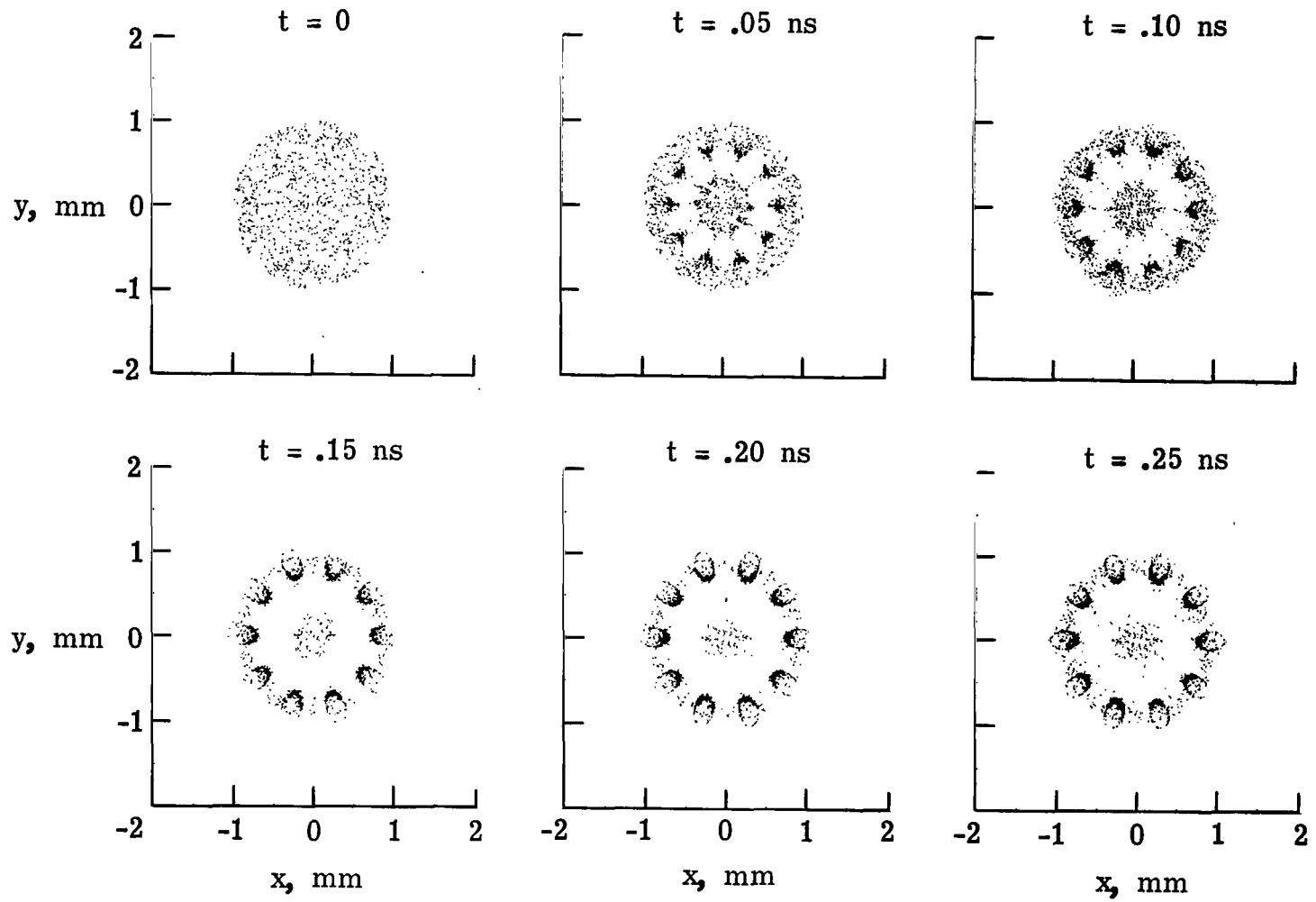


Figure 11.- Evolution of the x-y distribution of 3000 electrons for the current reduction phase of the filament model.

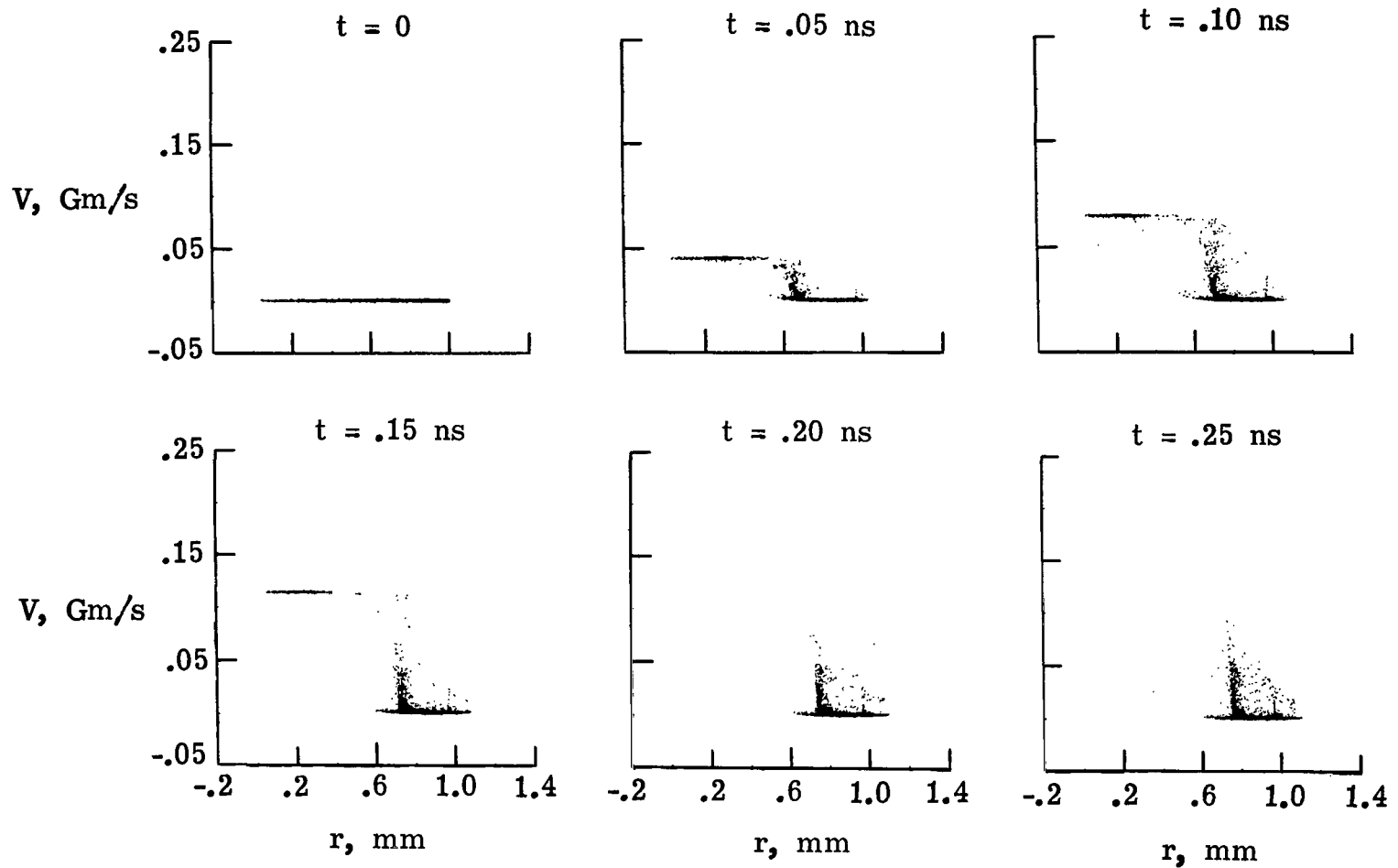


Figure 12.- Evolution of the distribution of 3000 electrons in  $V$ - $r$  space during the current reduction phase in the current filament model. Note that electrons with  $r < R$  undergo essentially free-streaming acceleration with considerable heating for electrons with  $r$  near  $R$ . The induced  $E_z$  is approximately equal to 6 MV/m in the central region.

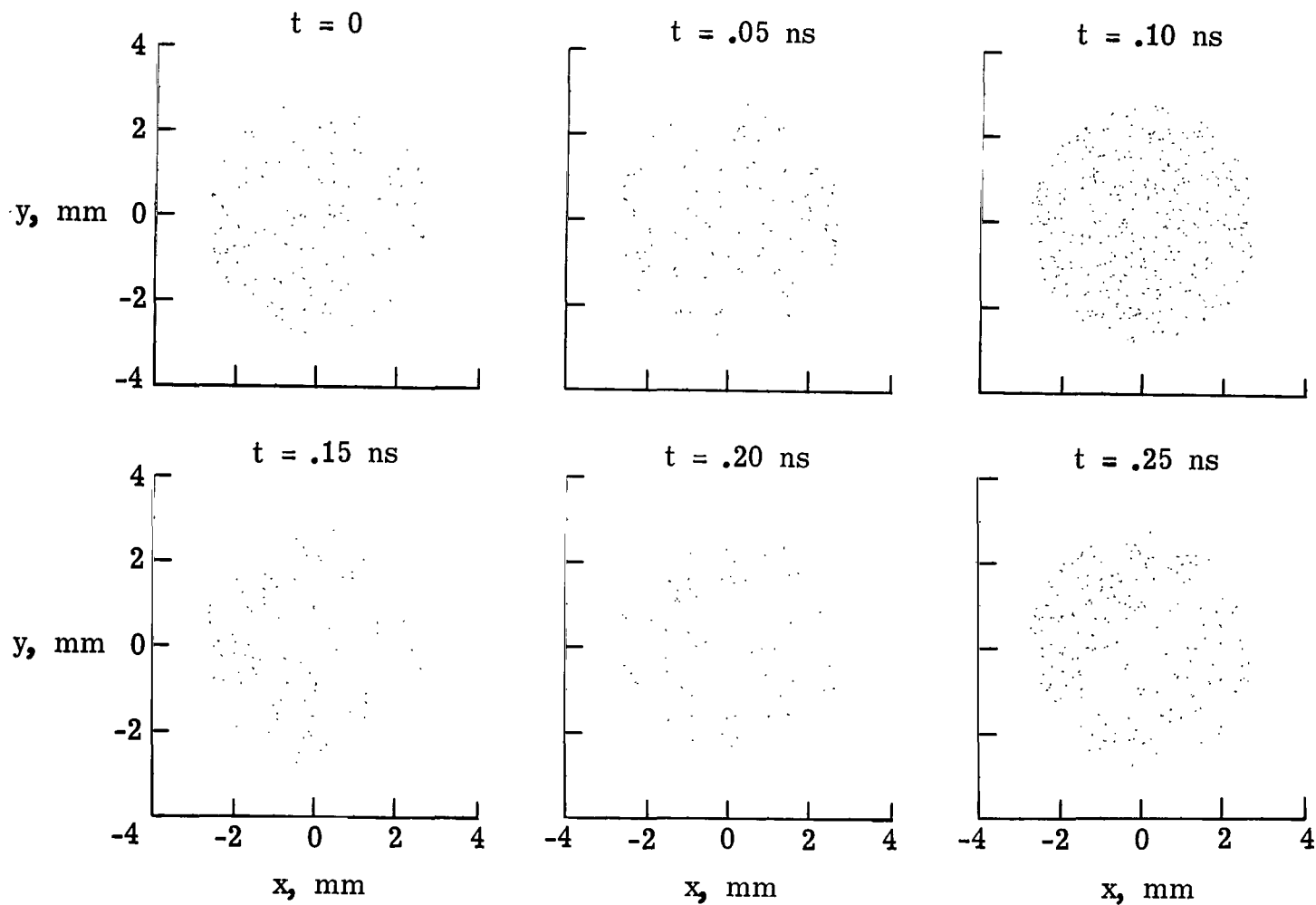


Figure 13.- Evolution of the spatial distribution of 3000 electrons during the compression phase for a uniform current distribution. The  $\vec{E} \times \vec{B}$  drift expels electrons from the central region.

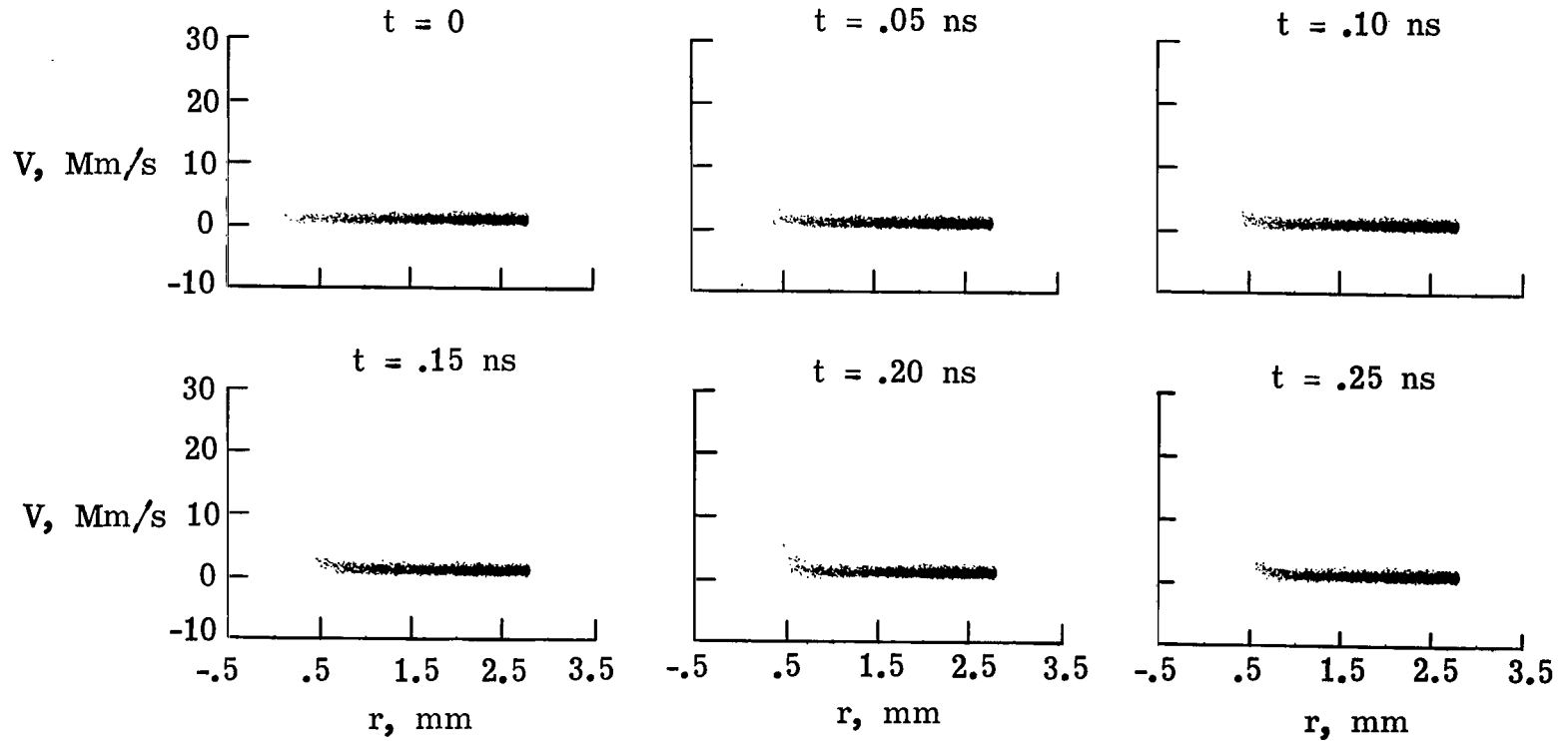


Figure 14.- Time evolution of 3000 electrons in  $V$ - $r$  space for the uniform current model. Electrons are expelled from the central region and are trapped by the strong magnetic field.

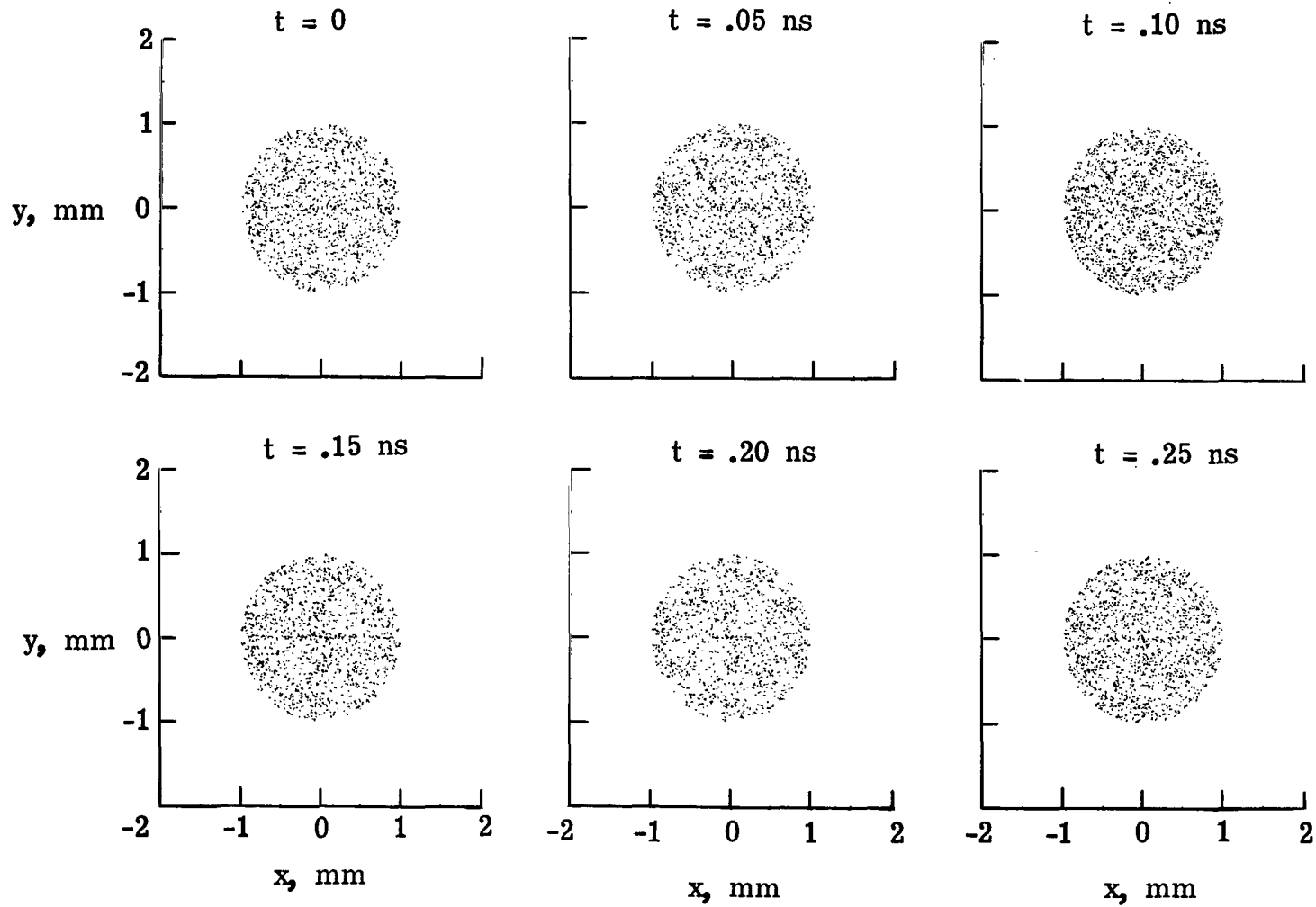


Figure 15.- Evolution of the spatial distribution of electrons in the current reduction phase of the uniform current model. Electrons are forced toward the axis by the  $\vec{E} \times \vec{B}$  drift.

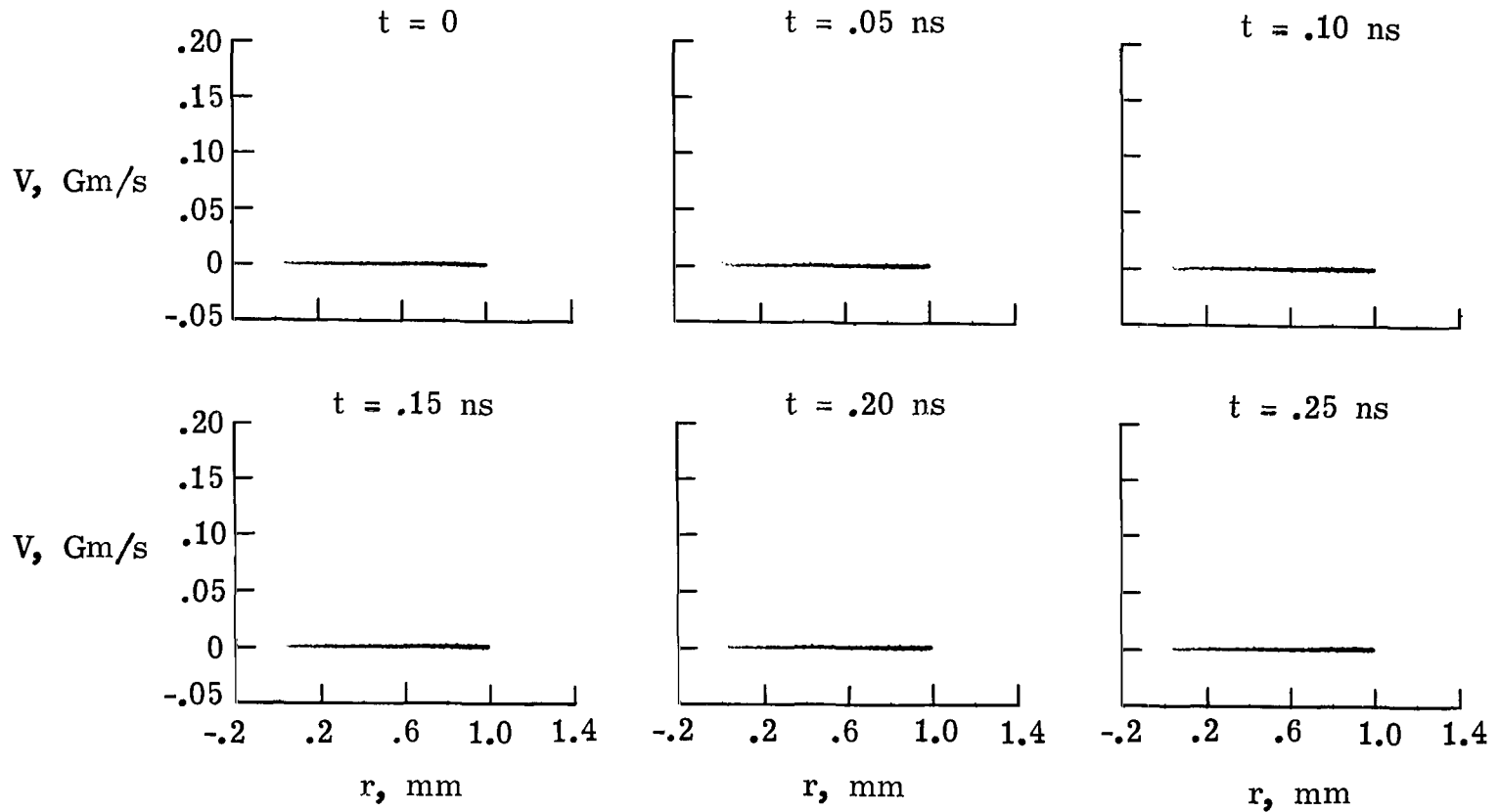
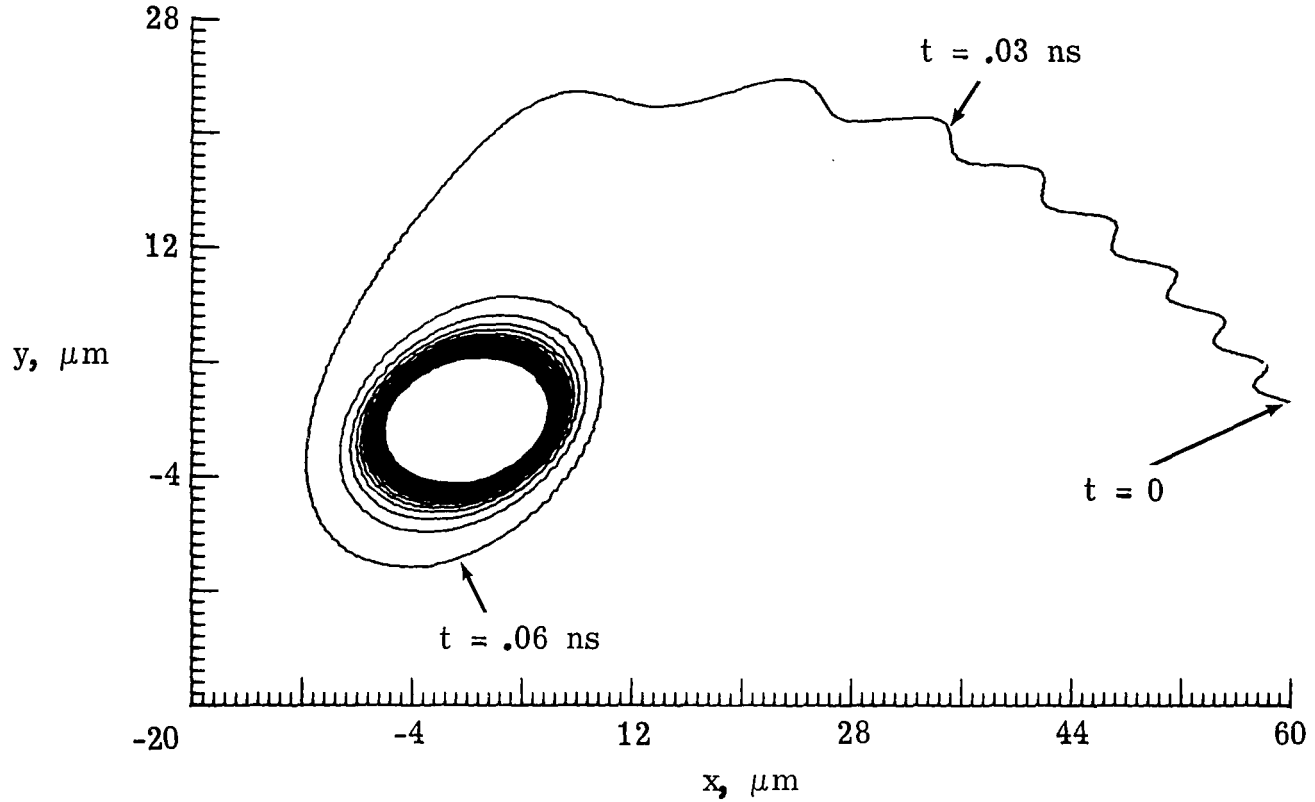
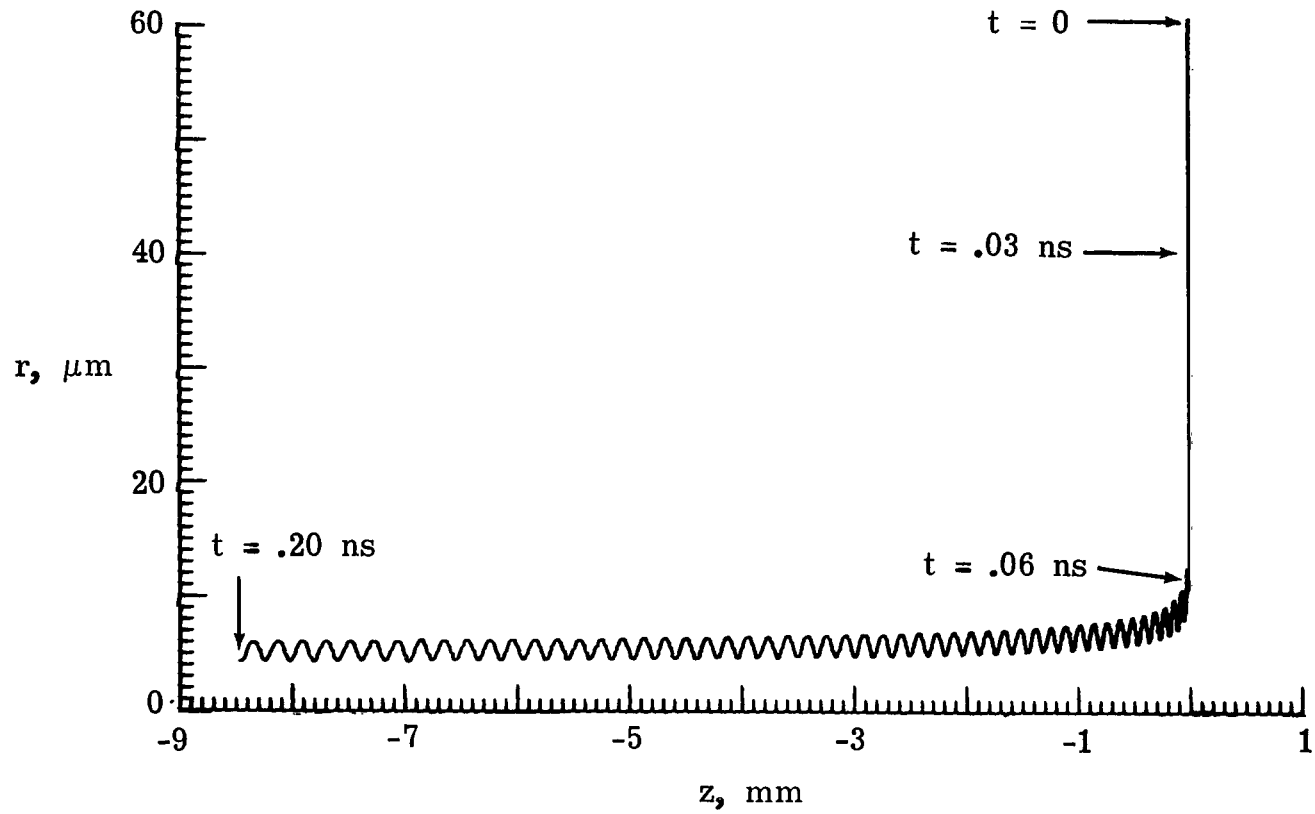


Figure 16.- Time evolution of the velocity of 3000 electrons as a function of radius. The  $\vec{E} \times \vec{B}$  drift now forces electrons toward the axis. Electrons away from the axis are tied to the magnetic field, whereas electrons within  $r_p$  of the axis are accelerated in the negative  $z$ -direction.



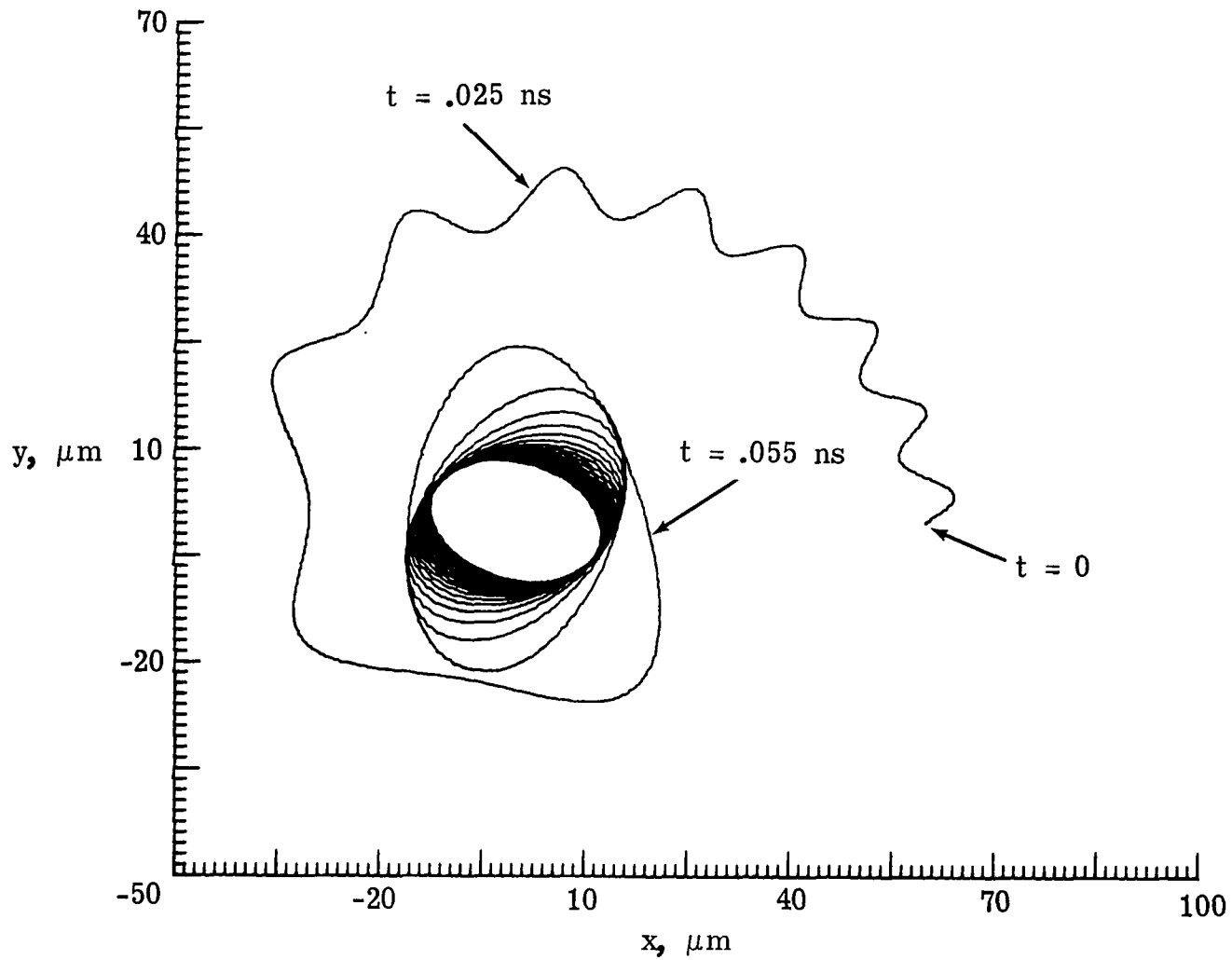
(a) Trajectory in x-y space.

Figure 17.- Typical electron trajectory near the central region during the current reduction phase in the uniform current model. Under the influence of the  $\vec{E} \times \vec{B}$  drift, the electron moves toward the axis. As the electron approaches within a Larmor radius of the axis, it is accelerated in the negative z-direction and "runs away."



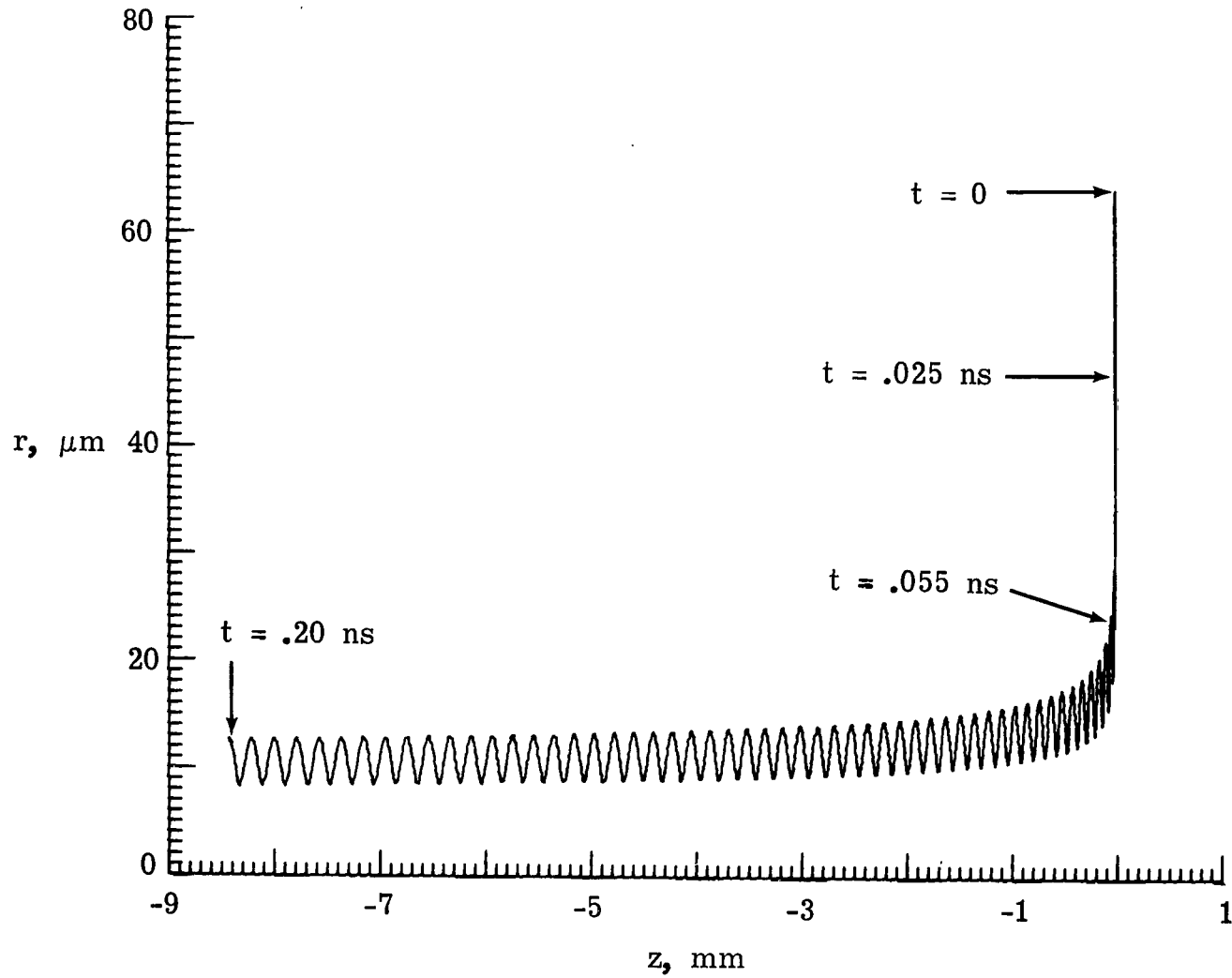
(b) Trajectory in  $r$ - $z$  space.

Figure 17.- Concluded.



(a) Trajectory in x-y space.

Figure 18.- Another example of a runaway electron.



(b) Trajectory in  $r$ - $z$  space.

Figure 18.- Concluded.

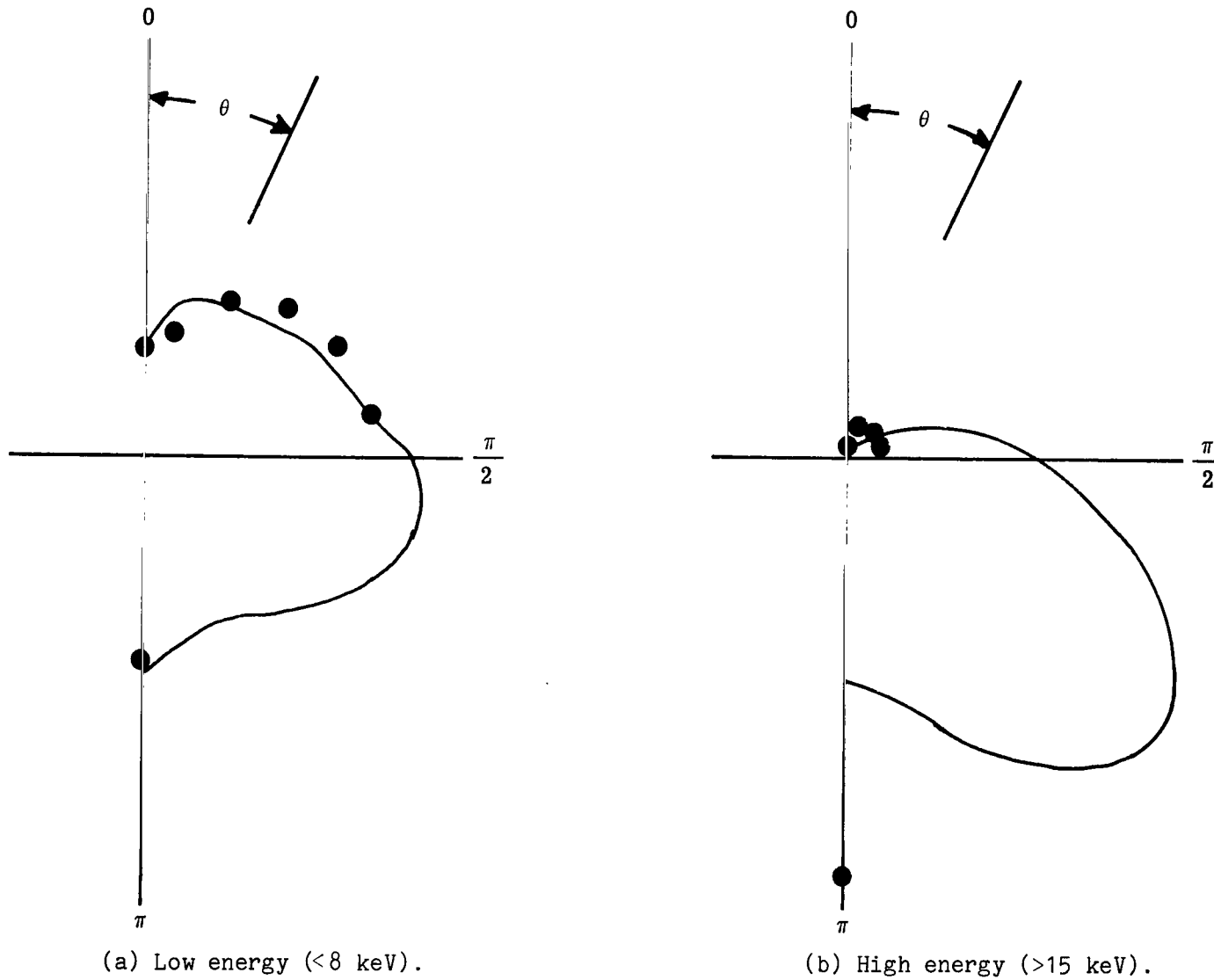


Figure 19.- Comparison of X-ray emission obtained from runaway electrons (solid curve) with experimentally determined X-ray emissions (dots) from the 25 kJ 20 kV plasma focus.



078 001 C1 U H 770128 S00903DS  
DEPT OF THE AIR FORCE  
AF WEAPONS LABORATORY  
ATTN: TECHNICAL LIBRARY (SUL)  
KIRTLAND AFB NM 87117

POSTMASTER : If Undeliverable (Section 158  
Postal Manual) Do Not Return

*"The aeronautical and space activities of the United States shall be conducted so as to contribute . . . to the expansion of human knowledge of phenomena in the atmosphere and space. The Administration shall provide for the widest practicable and appropriate dissemination of information concerning its activities and the results thereof."*

—NATIONAL AERONAUTICS AND SPACE ACT OF 1958

## NASA SCIENTIFIC AND TECHNICAL PUBLICATIONS

**TECHNICAL REPORTS:** Scientific and technical information considered important, complete, and a lasting contribution to existing knowledge.

**TECHNICAL NOTES:** Information less broad in scope but nevertheless of importance as a contribution to existing knowledge.

**TECHNICAL MEMORANDUMS:** Information receiving limited distribution because of preliminary data, security classification, or other reasons. Also includes conference proceedings with either limited or unlimited distribution.

**CONTRACTOR REPORTS:** Scientific and technical information generated under a NASA contract or grant and considered an important contribution to existing knowledge.

**TECHNICAL TRANSLATIONS:** Information published in a foreign language considered to merit NASA distribution in English.

**SPECIAL PUBLICATIONS:** Information derived from or of value to NASA activities. Publications include final reports of major projects, monographs, data compilations, handbooks, sourcebooks, and special bibliographies.

**TECHNOLOGY UTILIZATION PUBLICATIONS:** Information on technology used by NASA that may be of particular interest in commercial and other non-aerospace applications. Publications include Tech Briefs, Technology Utilization Reports and Technology Surveys.

**Details on the availability of these publications may be obtained from:**

**SCIENTIFIC AND TECHNICAL INFORMATION OFFICE**

**NATIONAL AERONAUTICS AND SPACE ADMINISTRATION**

**Washington, D.C. 20546**